INVESTIGATION OF ANTENNAS AND ENERGY HARVESTING METHODS FOR USE WITH A UHF MICROTRANSCEIVER IN A BIOSENSOR NETWORK

by

AMELIA LYNN HODGES

B.S., Kansas State University, 2010

A THESIS

submitted in partial fulfillment of the requirements for the degree

MASTER OF SCIENCE

Department of Electrical and Computer Engineering
College of Engineering

KANSAS STATE UNIVERSITY
Manhattan, Kansas

2013

Approved by:

Major Professor
William B. Kuhn

Copyright

Abstract

This work was a part of NASA EPSCoR Project NNX11AM05A: *Biosensor Networks and Telecommunication Subsystems for Long Duration Missions, EVA Suits, and Robotic Precursor Scout Missions*. The project's main goal is the development of a wireless sensor network inside an astronaut's spacesuit. Antennas are essential components in a wireless network. Since this antenna will be used inside the spacesuit it is important to consider both the physical size limitations and the desired antenna polarization. After exploring the WWVB radio station antenna which provides the preferred vertical polarization and has a suitable aspect ratio, the top hat antenna seemed promising for intrasuit communication. The design of a top hat antenna is outlined. Then, the antennas were tested using 433 MHz radios in a full scale model spacesuit. This spacesuit was designed specifically to model the behavior of aluminized mylar in the real suit. Test results support the feasibility of an intrasuit wireless network. If a gateway radio is placed on the chest or back, a sensor could be placed anywhere on the body and provide an adequate signal. These initial tests did not include a matching network, but the additional link-margin afforded by a matching network, even an imperfect match, is considered.

Energy harvesting is explored as an alternative to batteries powering the intrasuit radio. In the oxygen rich environment of a spacesuit, even the smallest spark can be catastrophic. A variety of energy harvesting options are explored with a focus on thermal energy harvesting. The temperature difference between the human skin and the astronaut's Liquid Cooling and Ventilation Garment can be used to produce a small voltage. To increase the voltage a step-up converter is implemented. Final integration of the two systems with a biosensor is left for on-going work in the three year NASA project.

Table of Contents

List of Figures

List of Tables

Acknowledgements

First, I'd like to acknowledge my major professor Dr. Kuhn. His insight helped to clarify issues as they occurred. It has been a privilege to work with him both through research and classes.

Thanks is also due to my committee members, Dr. Kuhn, Dr. Natarajan, and Dr. Warren. Their flexibly and patience made it possible for me to complete this work with limited stress.

I am appreciated of Mohammed Taj-Eldin and his work in parallel with my own. Thank you for determining what fabric should be used in the model suit. I am glad to know you will continue to expand on the signal propagation inside of the spacesuit.

Erin Monfort-Nelson also played an essential part in this research. Without the design and construction of the model suit we would not be able to understand the in-suit propagation as we now do.

Thanks to German Sanchez for contacting Perpetua and learning more about their TEGs. Also, thanks to the undergrad research team which will continue the antenna testing at other frequencies as well as continuing the TEG research.

Thanks to Xiongjie Dong for picking up the daughter board work, adding a sensor and making it a reality.

I'd also like to acknowledge NASA EPSCoR Project NNX11AM05A for funding this research and providing me an avenue to learn about the problems facing future astronauts.

These acknowledgements would be incomplete without mentioning my family and friends who have helped me survive the journey to my master's degree. Over my years at K-State I've been able to learn from many great professors and without those building blocks as foundation I never would have completed this thesis. But, without the support of my family and friends I would not have made it.

Dedication

This work is dedicated to the future engineers of the world. May your experiences inspire you to provide solutions to the world's problems, both big and small. Take the skills you acquire and use them to change the world. All the hard work and dedication will pay off.

Chapter 1 - Introduction

1.1 NASA EPSCoR Project NNX11AM05A

This work was a part of NASA EPSCoR Project NNX11AM05A: *Biosensor Networks and Telecommunication Subsystems for Long Duration Missions, EVA Suits, and Robotic Precursor Scout Missions*. In a cross-disciplinary effort, the Department of Kinesiology, the Department of Electrical and Computer Engineering, and the Electronic Design Laboratory at Kansas State University are working to design and implement a network of wireless biosensors for use in future space suits. The group's effort has been divided into five different tasks. Task one focuses on evaluating which physiological signals could be monitored to determine fatigue before it occurs. In addition, task one includes developing sensors to detect these physiological signals. Task two focuses on the radio environment within the space suit. Since spacesuits contain layers of radio opaque aluminized Mylar, the system is more complex than a normal body area network. In this task the space suit is modeled in three different ways: two physical models and one simulation model. Task three focuses on the network of sensors and how different transmit schemes can be effective. Task four focuses on furthering the development of the K-State micro-transceiver built under a previous NASA project. Task five focuses on the nontechnical aspect of outreach to undergraduate researchers, K-12 students, and the general public. This thesis work primarily relates to task two and task four; however, it is the foundation for the development of a daughter board that will incorporate the work of the first four tasks.

1.2 Thesis Goals and Motivation

The first goal of this work is the development of an antenna to be used in the spacesuit. Antennas are designed based on the frequency or frequencies they will transmit and/or receive. Their size is derived from the wavelength. Since this work focusses on bio-signals, the frequencies of interest are in the Medical Device Radiocommunications Service (MedRadio) band ranging from around 400 to 450 MHz—with some frequencies excluded [1]. The wavelength ranges from 67 cm to 75 cm, so that even at a quarter wavelength a distance of 17 cm to 19 cm would be required. Thus normal quarter or half wavelength antennas are too big for in-suit use. Other less traditional antennas needed to be explored. Many researchers are working

to develop compact antennas for use in healthcare and many other operations requiring small antennas [2, 3, 4]. This research hopes to provide one possible solution.

The second goal of this work is understanding the in-suit propagation of signals using the antenna and relates directly to the goals of task two. This study was a collaborative effort between the author and another graduate student. Two physical models were developed. The first was a small scale model consisting of a large aluminum duct. The second was a full scale model made from conductive fabric.

The third goal for this work is replacing batteries with a safer energy harvesting alternative. The energy harvesting alternative would also not require regular replacement [5, 6, 7, 8]. Energy harvesting uses energy available in the environment and converts it to a more useful form. This work involved surveying available options and determining what could be used inside the suit. In addition, devices are tested and their performance evaluated.

The fourth and final goal of this work is integration of an antenna, energy harvesting and a bio-sensor onto a single daughter board to be used with the radio in task four. This would create a compact system which could provide both NASA and terrestrial doctors a way to remotely monitor clients' health.

This thesis steps through the work to complete these four goals. The first three are given their own chapters while the fourth is discussed in the continuing/future work section.

Chapter 2 - Designing an Antenna and Matching Network

2.1 Background Study of Antennas

2.1.1 Antennas Options

Antennas come in all shapes and sizes [2, 9, 10, 11]. The most basic are the halfwave dipole and the quarterwave monopole. The current in a halfwave dipole induces a magnetic field wrapping around the radiating element and induces an electric field between the radiating elements. The quarterwave monopole behaves similarly, with the ground plane functioning as the second radiating element. The loaded monopole is a shortened quarterwave monopole with an inductor built into the antenna, thus compensating for the increase in capacitance caused by shortening the monopole. The patch antenna's behavior is also comparable to the halfwave dipole. A simple model is two dipoles on parallel edges of the patch. The biggest difference between these three antennas and the halfwave dipole is their radiation pattern. The halfwave dipole is nearly isotropic with a directivity of only 2dBi (dB above isotropic) while the other three have about 3dB of directivity gain, since the signal radiates in only one hemisphere, above the ground plane [9].

The following table outlines some of the characteristics of these antennas as well as two others: small loop and top hat. These two antennas are less similar to the dipole than the previously mentioned antennas. The small loop antenna is best thought of as an inductor since it primarily couples to the magnetic field as opposed to the electric field. The top hat is examined further in later sections and seemed the most promising for use inside the space suit.

The advantages and drawbacks expressed in table 2.1 address some on the requirements of in-suit antennas. The following section outlines these requirements and evaluates the antennas for potential use in the suit.

Type	Advantages	Drawbacks
Quarterwave Monopole	Well understood Simple design characteristics	Physical size
Halfwave Dipole	Well understood Simple design characteristic	Physical size
Loaded Monopole [11]	Similar to monopole but with inductive loading to reduce height	Orientation requirements Physical size
Patch [4,10]	Two dimensional Could be placed directly on body	Orientation requirements Space requirements Usually high frequency
Small Loop	Two dimensional Used in frequency range	Low efficiency Orientation requirements
Top Hat Antenna [12,13,14]	Physically small for wavelength Easy to integrate with current ratio	Not well understood No design characterization

Table 2.1 Antennas and Some Basic Characteristics

2.1.2 Requirements of In-Suit Antennas

This antenna is being developed for use inside a space suit. Such an environment limits the type of antennas that can be used. The traditional halfwave dipole and quarterwave monopole are impractical since the space in the suit is smaller than the 17 cm to 19 cm required for a quarterwave antenna in the MedRadio band. Even if the physical height was reduced by using a coil instead of a straight wire, the height would still be large enough (2-3 cm) to interfere with the spacesuit. A loaded monopoles height would be between 3 and 17 cm, while the inductive load reduces the height the nature of a monopole requires more height then desired for intrasuit applications. Because of their physical size, these antennas can quickly be eliminated.

In addition to size restriction, polarization must be considered. Ideally the field would propagate parallel to the human body with a vertical polarization. In this discussion it is assumed that the antenna will be placed on the arm; however, the arm could be replaced by any other part of the body. The small loop and patch antennas are polarized in the plane of the antenna. To minimize the antennas interference with the space suit the small loop and patch antennas should be placed so the antenna's plane is parallel to the arm (figures 2.1). With this orientation, the

antennas are horizontally polarized. To create the desired propagation the antennas must be perpendicular to the arm (figure 2.2). In this orientation the antennas' physical size becomes larger than the space available in the suit, leaving only the loaded top hat for potential use in the spacesuit. When this antenna is placed on the arm the electric field is vertically polarized and the signal propagates parallel to the arm. The physical size of the top hat antenna is also small enough to not impede the astronaut's ability to where the suit. The following section features a study of a well-known top hat antenna.

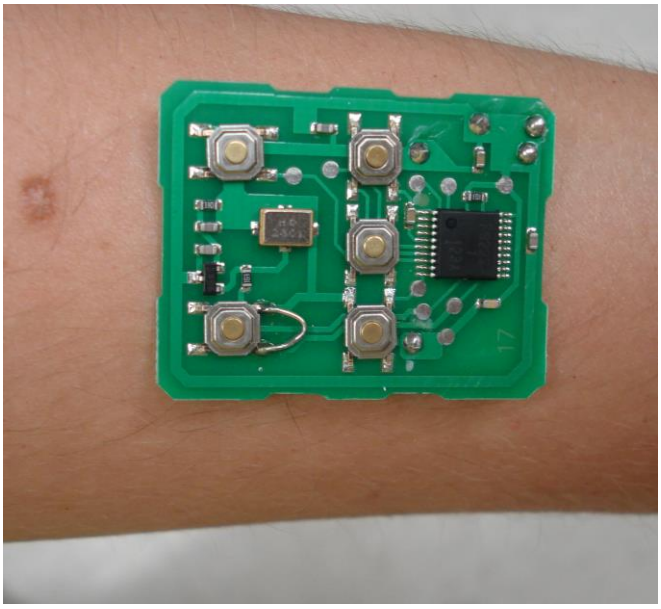

Figure 2.1 Small Loop Antenna Parallel to Arm (Birdseye View)

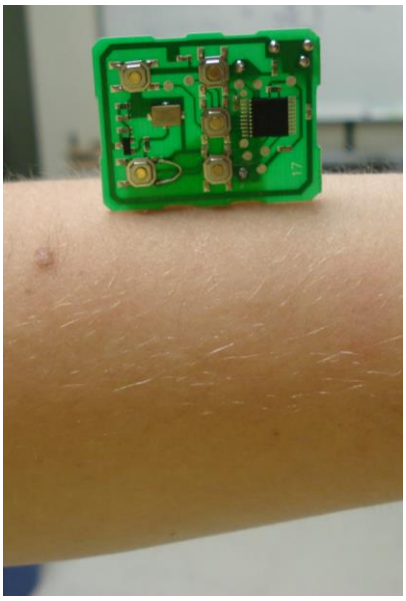

Figure 2.2 Small Loop Antenna Perpendicular to Arm (Side View)

2.1.2 WWVB Antenna

WWVB, in Fort Collins, Colorado, transmits time code at 60 kHz and has done so since 1956. At that frequency the wavelength is nearly 5 km, thus a quarter wavelength would be 1.25 km. The actual height of the WWVB antenna is 122 m or 1/40 of a wavelength [14]. By using capacitance and extending the antenna vertically, the WWVB antenna (figure 2.3) is able to have an electrically short post. Four towers, in a diamond shape, support a heavy cable system that creates the capacitive hat. The top hat has an area of 65,497 m^2 [15]. Radials were placed in the

ground to improve its conductivity, thus creating more capacitance between the two planes and reducing losses from the ground system currents.

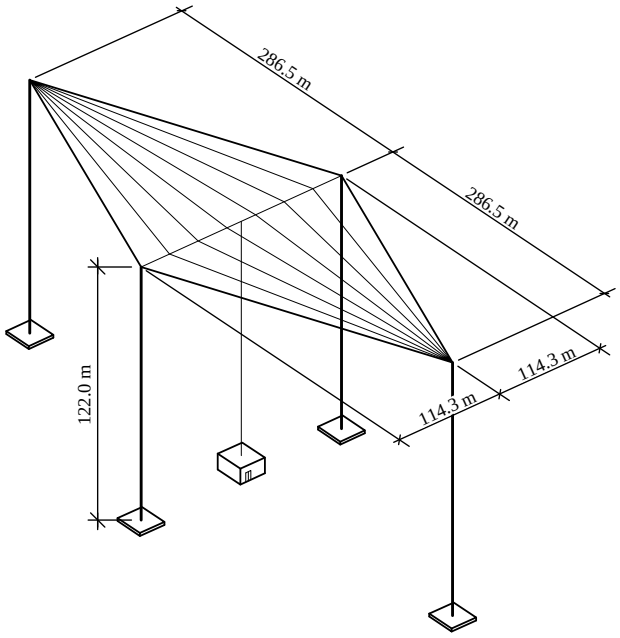

Figure 2.3 WWVB Antenna Sketch

If this antenna can be scaled down to the 400 MHz wavelength of 75 cm the resulting antenna would easily fit insides the spacesuit. Using a scaling factor found from the ratio of wavelengths (0.75m/5000m), the height would be 1.8 cm. Scaling the area based on the square of the wavelength would result in 15 cm^2area. Such a small antenna is ideal for intra-suit use, providing the desired vertical polarization in a size comparable to a typical wristwatch.

2.2 Designing the Top Hat Antenna

2.2.1 Components of Top Hat Antennas

A top hat antenna consists of three basic components: a ground plane, an electrically short post, and a capacitive top hat. The post is considered electrically short because it is short relative to the wavelength. The top hat antenna has an excitation point between the ground plane and the electrically short post. On the end opposite the excitation point the post is connected to the top hat. The top hat serves two functions. The first is a vertical elongation of the antenna

like the inverted L monopole. The second is the capacitance between the top hat and ground plane.

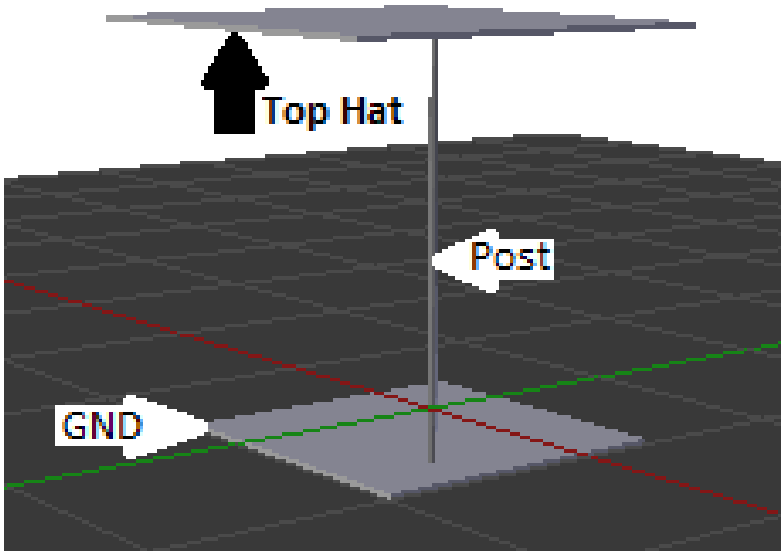

Figure 2.4 Top Hat Antenna with Components Labeled

2.2.2 Procedure for Simulation

Each of the three components plays a key role in the antenna's function. Unlike many other antennas there are no set rules or design equations for top hat antennas. To gain a better understanding of how each parameter affects the return loss, S_{11}, of the antenna, we implemented simulations using Agilent's ADS software. Ideally S_{11} would have a large resistive component to maximize power transmitted. It would also have a small reactive value so a smaller, lower Q circuit could be used for wide-bandwidth matching. The following section elaborates on each component's role in determining S_{11} while Appendix A details the procedure for setting up the simulation.

2.2.3 Understanding Each Components' Role

Each of the three components is analyzed individually with the other two components held constant. The general pattern remains the same regardless of our two test scenarios—round top hat with post in center vs. rectangular top hat with post off center. Standard values for the

round top hat scenario were 1000 mil top hat diameter, 150 mil post diameter and 500 mil post height.

2.2.3.1 Adjusting Post Height

Simulations were conducted as described in Appendix A of this thesis. We used 75 mil step size and centered measurement on the standard value, 500 mil post height. Test values range from 275 mil to 725 mil. Only FEM results were recorded. Values are based on a 400 MHz simulation frequency and Z_0 = 50 Ω. The table below shows the results. Two graphs are also presented to provide a visualization of the trends.

Adjusting Post Height	FEM Z_{ant}		Cap value
	Real	Imaginary	
275 mil	0.165	-153.08	16.33 pF
350 mil	0.236	-160.258	15.60 pF
425 mil	0.313	-162.86	15.35 pF
500 mil	0.402	-165.565	15.10 pF
575 mil	0.5	-165.412	15.11 pF
650 mil	0.601	-166.111	15.05 pF
725 mil	0.721	-165.409	15.11 pF

Table 2.2 Effect of Changing Post Height on Real and Imaginary Terms of the Antenna Impedance

From figure 2.5 we see that post height has a positive correlation with R_{ant}. As one increases so does the other. This agrees with the understanding of resistance; however, it is important to note that R_{ant} is the sum of two distinct resistances: the radiation resistance R_{rad} and the physical resistance R_{phy}. Equation 2.1 expresses the relationship between length and physical resistance. In this case the length is the height of the post as well as a small portion of the dimensions of the top hat.

$$R_{phy} = \rho \frac{L}{A} \qquad (2.1)$$

In this equation R_{phy} is the physical resistance, ρ is the resistivity of the wire, L is the length (height) of the wire, and A is the conductive area of the wire. Recalling that neither the area nor the resistivity changed leaves a directly proportional relationship between physical resistance and height. This matches with the simulation results to a first order. However, if the 0.165 Ω resistance at 275 mils height is scaled to 725 mils, the value would be 0.435 Ω. The difference between the simulated value and the scaled value (0.721 Ω - 0.435 Ω = 0.286 Ω) can be taken as

an estimate of radiation resistance component, R_{rad}. Assuming the simulations are correct, even the 275 mil post height has a radiation resistance. The ratio of R_{rad} to R_{ant} increases with post height. Thus the taller post results in a more efficient antenna.

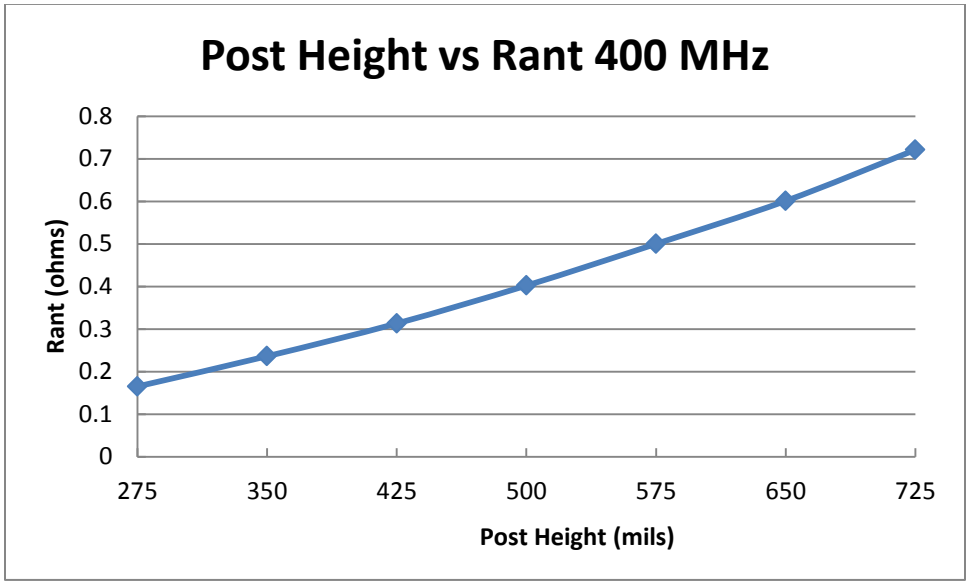

Figure 2.5 Graph of Post Height Effect on R_{ant}

From the second graph it is easily inferred that post height has a positive correlation with $|X_{ant}|$. This means that as the post height increases the capacitance decreases. Recall the equation for a parallel plate capacitor.

$$C = \varepsilon_r \varepsilon_o \frac{A}{d} \qquad (2.2)$$

With C being the capacitance, ε_r the relative permittivity, ε_o the electric constant, A the overlap area, and d the distance between the plates. If $\varepsilon_r \varepsilon_o$ and Area are held constant (which is true in these simulations) while the distance is increased, then the capacitance should decrease. In theory, if the distance between the plates is twice as large the capacitance should be half as large. In simulations, post height is increased nearly 3 times with the capacitance varying by just over 1 pF. Possible explanations are parasitic capacitance from the post and increasing inductance offsetting the capacitance change. Figure 2.8 illustrates the basic concept. As the post becomes taller its effective area is increased. While it is not a parallel plate there is still a small capacitance between each plate and the post. As the area of the post increases the capacitance to

both plates will also increases (though not as drastically as for parallel plates). This increase is most likely partly responsible for the net reduction in capacitance being smaller than expected.

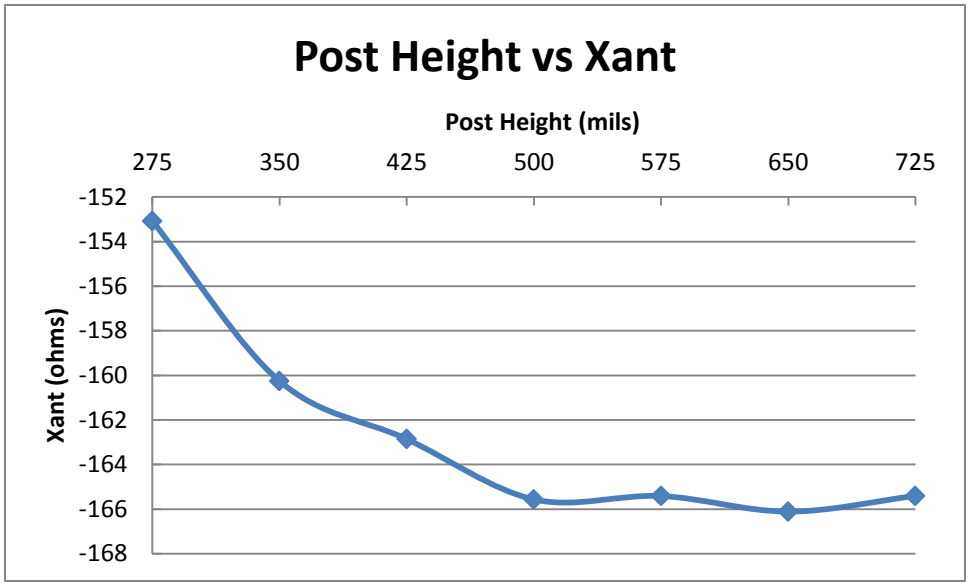

Figure 2.6 Graph of Post Height's Effect on X_{ant}

Increasing the post height is both beneficial and unfortunate. A taller post provides the desired large ratio of radiation resistance to physical resistance thus improving the efficiency. Unfortunately, increased post height increases the magnitude of reactance. For matching purposes reactance should be small. Since the advantage of greater efficiency outweighs the disadvantage of the increased mismatch, the post height should be maximized. Further consideration must be made for physical limitations when implemented in conjunction with the existing radio board and inside the spacesuit.

2.2.3.2 Adjusting Post Diameter

In simulating change versus post diameter, a 40 mil step size was used (with one 50 mil step), centered on the standard 150 mil post diameter. Test values range from 20 mil to 270 mil. The radius is included because it is the value used in simulation. Only FEM results were recorded. Values are based on a 400 MHz simulation frequency and Z_0 = 50 Ω. The table below shows the results. Two graphs are also presented to provide a visualization of the trends.

Adjusting Post Diameter & Radius		FEM Z_{ant}		
		Real	Imaginary	Cap value
20 mil	10 mil	0.96	-249.7	10.01 pF
60 mil	30 mil	0.751	-224.802	11.12 pF
100 mil	50 mil	0.578	-198.46	12.60 pF
150 mil	75 mil	0.402	-165.565	15.10 pF
190 mil	95 mil	0.322	-147.948	16.90 pF
230 mil	115 mil	0.244	-128.456	19.46 pF
270 mil	135 mil	0.185	-110.215	22.68 pF

Table 2.3 Effect of Changing Post Diameter on Real and Imaginary Terms of the Antenna Impedance

The first graph shows how the resistance of the antenna is affected by changing the post diameter. There is a negative correlation between the two since the resistance decreases as the post diameter increases. As explained in the previous section, the antenna resistance (R_{ant}) is the sum of the radiation resistance (R_{rad}) and the physical resistance (R_{phy}). The radiation resistance can be assumed to remain the same since the electromagnetic field is not strongly affected by the diameter of the post; however, the physical resistance changes. Equation 2.3 is used in conjunction with equation 2.1 to express the relationship between diameter and physical resistance.

$$A = \pi D \delta \qquad (2.3)$$

In this equation A is the conductive area of the wire, D is the diameter of the wire, and δ is the skin depth of the material at the frequency of operation. Concentrating on equation 2.3, π and skin depth (δ) remain constant for a given material at a constant frequency therefore the area is directly proportional to the diameter. As the diameter increases so will the area. Referring back to equation 2.1 and recalling that neither the length nor the resistivity changed leaves an inverse relationship between resistances and area. Combining the two equations, diameter become inversely proportional to resistance thus as diameter increases resistance decreases. This matches with the simulation results to a first order. However, if the 0.96 Ω resistance at 20 mils is scaled to 270 mils, the value would be 0.071 Ω. The difference (0.185 Ω - 0.071 Ω = 0.11 Ω) may be taken as an estimate of the constant radiation resistance component R_{rad}. In this case, the 270 mil post provided a much larger ratio of R_{rad} to R_{ant}, and an efficiency greater than 50%.

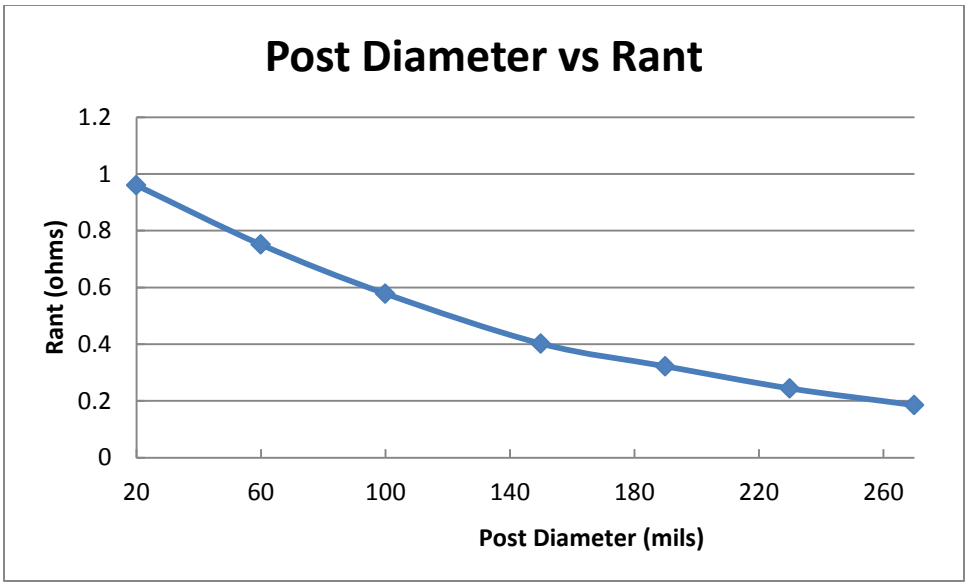

Figure 2.7 Graph of Effect of Post Diameter on R_{ant}

The second graph also shows a negative correlation between post diameter and the magnitude of reactance. As post diameter increased, the magnitude of reactance decreases. As the post diameter increases the fringe capacitance from the post increases and adds to the net capacitance. Since capacitance is inversely proportional to reactance, the reactance magnitude will decrease while the capacitance increases. Figure 2.8 illustrates this concept.

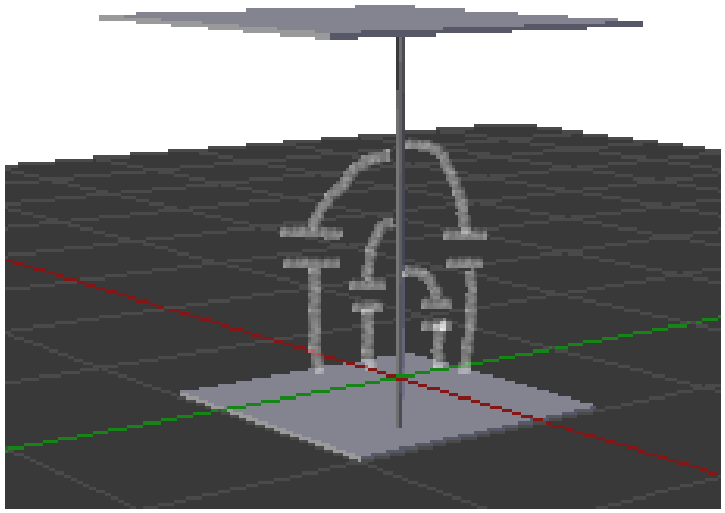

Figure 2.8 Illustration of Fringe Capacitance

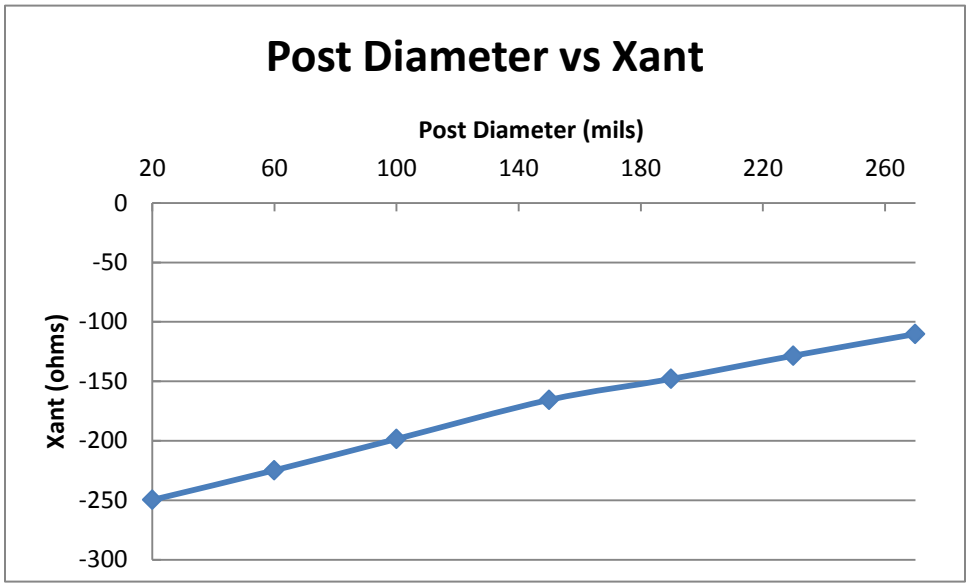

Figure 2.9 Graph of Effect of Post Diameter on X_{ant}

A larger post diameter results in the desired effect. The ratio of radiation resistance to physical resistance increases with the post diameter. Efficiency is improved. For reactance the larger post diameter decreases the magnitude thus decreasing the mismatch. A smaller reactance results in a smaller inductor needed to cancel the capacitance.

2.2.3.3 Adjusting Top Hat Diameter

To determine top hat diameter's effect a 100 mil step size was used and measurements centered on the standard value, 1000 mil top hat diameter. Test values ranged from 500 mil to 1500 mil. Only FEM results were recorded. Values are based on a 400 MHz simulation frequency and Z_0 = 50 Ohms. The table below shows the results. Two graphs are also presented to provide a visualization of the trends.

Adjusting Top Hat Diameter & Radius		FEM Z_{ant}		Cap value
		Real	Imaginary	
500 mil	250 mil	0.184	-242.197	10.32 pF
600 mil	300 mil	0.232	-227.795	10.97 pF
700 mil	350 mil	0.276	-210.575	11.87 pF
800 mil	400 mil	0.321	-194.663	12.84 pF
900 mil	450 mil	0.365	-179.767	13.91 pF
1000 mil	500 mil	0.402	-165.565	15.10 pF
1100 mil	550 mil	0.444	-154.989	16.13 pF
1200 mil	600 mil	0.472	-141.387	17.68 pF
1300 mil	650 mil	0.51	-131.367	19.03 pF
1400 mil	700 mil	0.537	-121.458	20.58 pF
1500 mil	750 mil	0.571	-111.042	22.51 pF

Table 2.4 Effect of Changing Top Hat Diameter on Real and Imaginary Terms of the Antenna Impedance

The first graph shows a positive correlation between top hat diameter and the antenna's resistance. As the top hat diameter increases the antenna's resistance also increases. This is consistent with theory. The increased top hat diameter creates a larger area capacitance and thus higher current in the post. This resistance is almost entirely physical resistance.

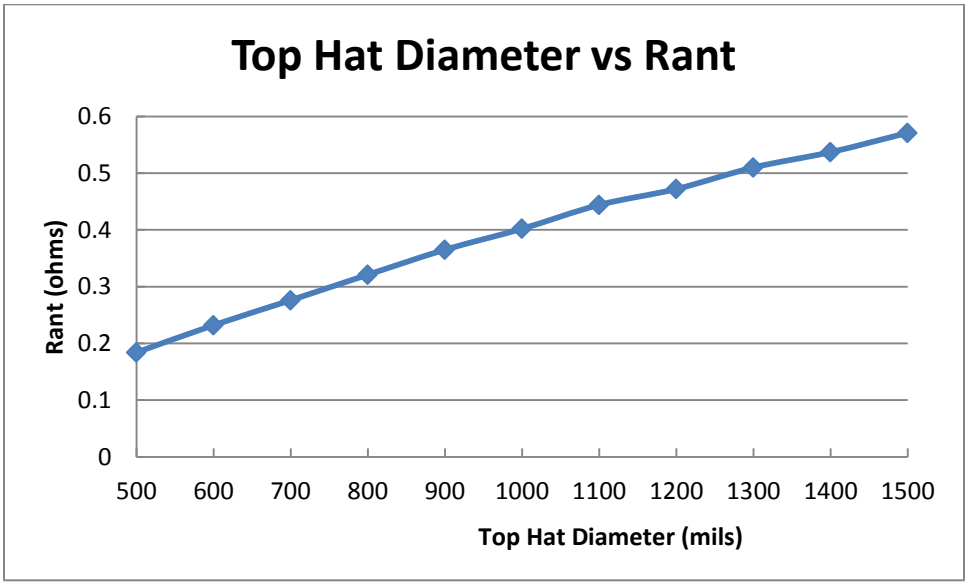

Figure 2.10 Graph of Effect of Top Hat Diameter on R_{ant}

From the second graph we see a negative correlation between top hat diameter and the magnitude of the antenna's reactance. An increase in top hat diameter results in a reduction of the antenna reactance magnitude. Theory matches well to this scenario. If we refer back to equation 2.2 for a parallel plate capacitor we see that the capacitance is directly proportional to the area of parallel plate overlap. Increasing the diameter will increase the overlap area and thus increase the capacitance. A larger capacitance means a smaller magnitude of reactance since it is inversely proportional to capacitance.

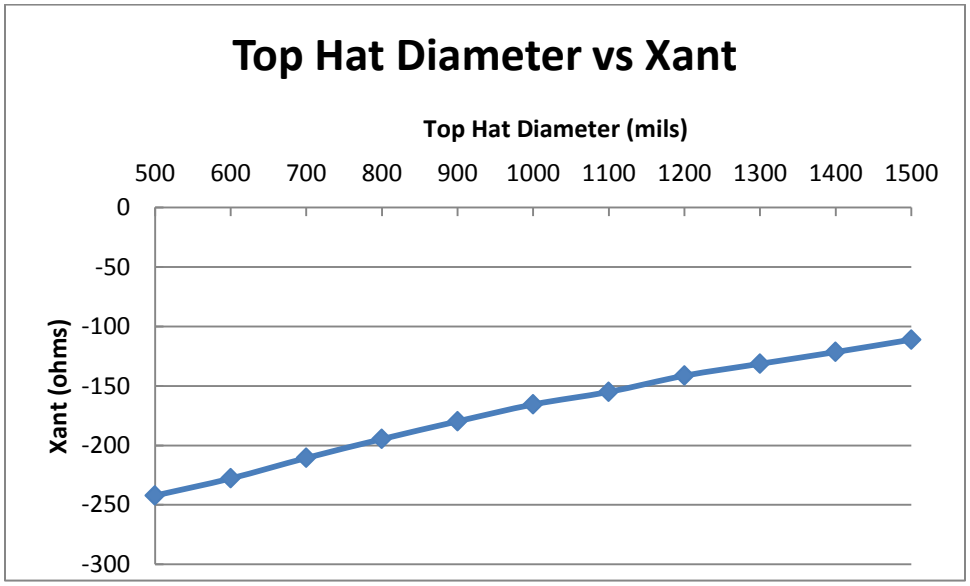

Figure 2.11 Graph of Effect of Top Hat Diameter on X_{ant}

Increasing the top hat diameter increases the resistance and reduces the reactance magnitude. However, physical constraints make it impossible to make the antenna very large. As mentioned in Chapter 1, the goal is to integrate with antenna with a radio board which provides a limit to the size of the top hat.

2.2.4 Final Design

Since we intend to use this antenna with a radio designed under the same EPSCoR project, it is important to consider the physical constraints. There are a few major factors in the antenna development that depend on the board. The radio board has a designated antenna pad. The antenna post must be placed at this point. The board is also limited in size so the top hat

cannot exceed the size of the board. Furthermore the radio board has a connector which provides a mechanical connection to the daughter board. In addition, this antenna daughter board will be used for other circuitry and the connector will transport electrical signals between the two boards. The connector also sets the distance between the two boards and thus determined the post height. For more information about the K-State radio board see Appendix B**.**

To make the antenna work in this environment we had to change the basic shape from a circular top hat to a rectangular top hat. The post also had to be moved from the center to the same location as the radio board. Before shipping the layout to be fabricated we simulated with the new layout and found the basic characteristics to be constant regardless of post placement and the top hat shape. For our final design we use ¾ and ½ of the radio board for the top hat and place the antenna on the left edge of the board. Figure 2.12 shows the board layout.

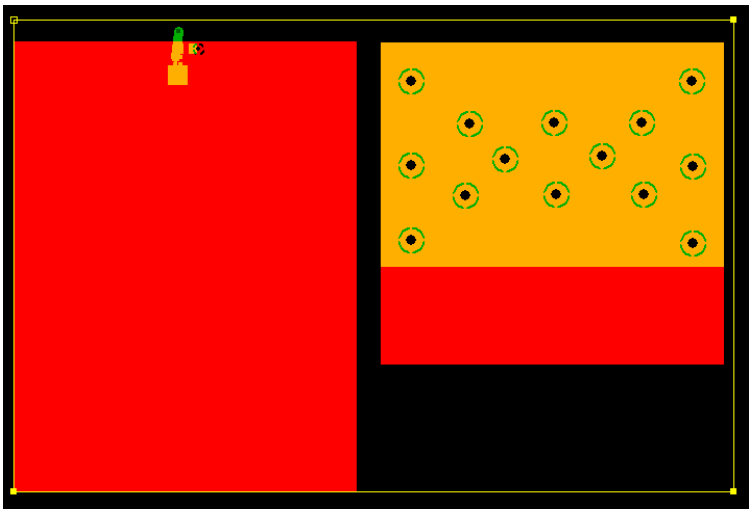

Figure 2.12 Layout of Prototype Antenna Board before Cutting into two Halves

This layout is cut in half and represents two boards. The left board is representative of the radio board. The red layer is the ground plane in the radio board and the yellow is for the antenna post connection as well as an SMA for testing the antenna. The right side of the board is the top hat. The yellow side connects to the post and is connected to the larger red plane with thermal vias. The final antenna is show in Figures 2.13 and 2.14.

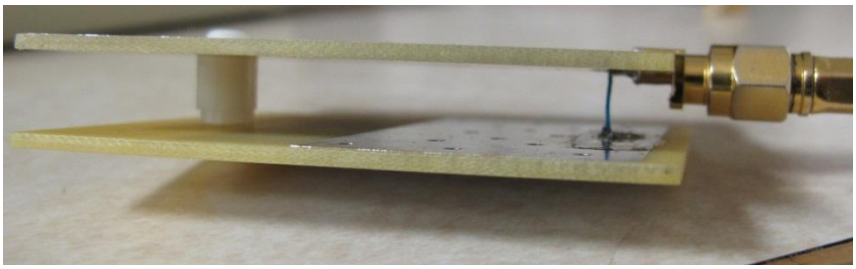

Figure 2.13 Side View of Inverted Top Hat Antenna

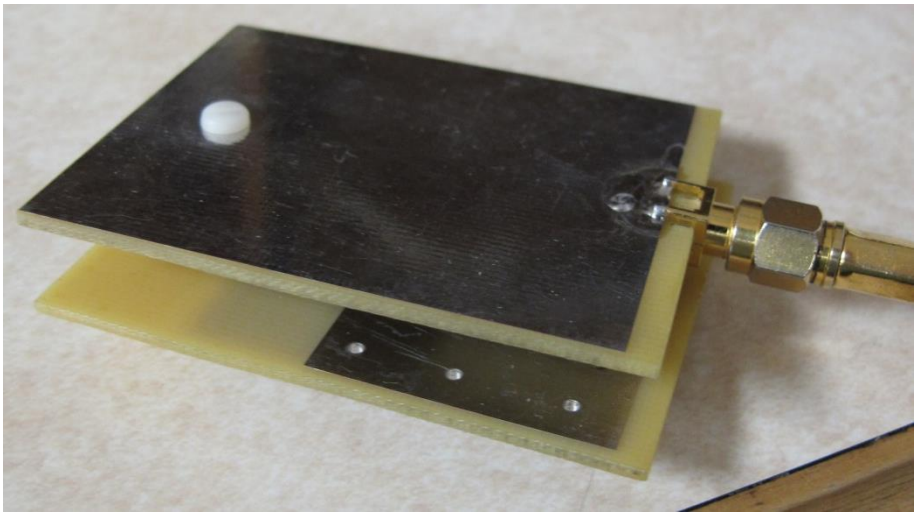

Figure 2.14 Bottom View of Top Hat Antenna

2.3 Determining Matching Network Parameters

It is well known that for an antenna to have maximum efficiency its impedance must be matched. In this case we know the antenna will have capacitance as well a resistance less than the desired 50Ω. To match we will use an L matching network, see figure 2.15. In this case the antenna resistance, R_{ant}, represents R_s, the output impedance of the radio board, $R_{out_{board}} = 50\ \Omega$, represents R_p, and the reactive values, X_s and X_p are inductive and capacitive respectively. The placement of the inductor and capacitor are done in order to reduce components since an inductor (X_1) is needed to cancel the antennas capacitance. These two inductors (X_s and X_1) can be combined and a single inductor used.

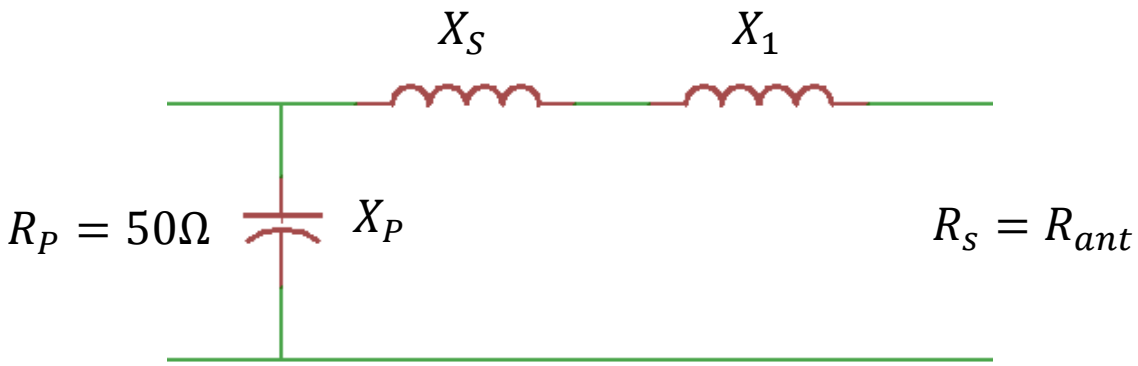

Figure 2.15 L Matching Network for Top Hat Antenna

Initial calculations were made based on the value of Z_{ant} found in simulations and the following equations:

$$q = \sqrt{\frac{50}{R_{ant}} - 1} \tag{2.4}$$

$$X_s = qR_{ant} \tag{2.5}$$

$$X_p = -\frac{1+q^2}{q^2}X_{ant} = -\frac{50}{q} \tag{2.6}$$

At 433 MHz, Z_{ant} was found to be 0.133 – j41.976 in Momentum simulation and 0.779 – j30.654 in FEM simulation. These values are based on the final antenna design characteristics and will provide a base line to be compared with measured values which were quite different due to presence of the body.

2.3.1 Initial Measurements

The impedance values below were found using an HP8753A/C Vector Network Analyzer. The top hat was placed on the surface with the large flood plane exposed to free space (figure 2.16) . The following table contains a set of measured values.

Test condition	Z_{ant} at 400 MHz		Z_{ant} at 433 MHz		Z_{ant} at 450 MHz	
	R (Ω)	X (Ω)	R (Ω)	X (Ω)	R (Ω)	X (Ω)
free space	11.3	-58.3	4.3	-48.0	3.4	-43.2
on arm	26.1	-35.3	15.5	-27.0	12.3	-23.8
on gnd plane	94.6	-27.1	24.6	-55.4	13.1	-42.8

Table 2.5 Z_{ant} at Three Frequencies under Three Test Conditions

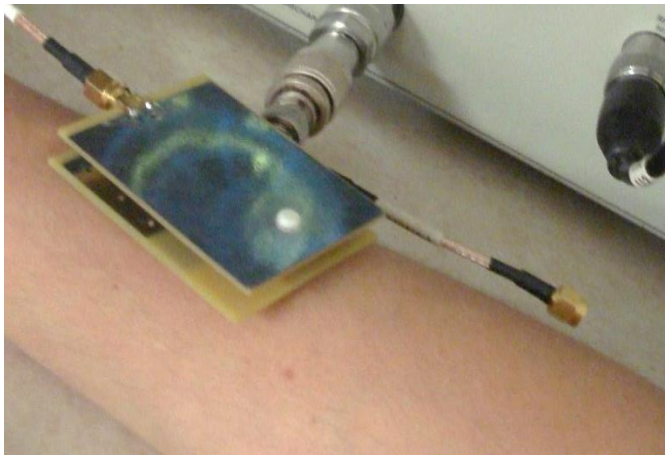

Figure 2.16 Antenna Placement on Arm

It is interesting to note that regardless of the top hat's contact surface, the antennas resistance and reactance decreases dramatically with an increase in the frequency. Also both resistance and reactance increase significantly as the top hat transitions from free space to arm to a ground plane.

It is important to compare these values back to the simulations. Since simulations were done only at 433 MHz, only those values will be compared. In each simulation the resistance is less than one ohm. The free space measurement is the closest to 1 but is still about 10 times larger than the simulated values. This difference is cause for suspicion. Initially we concluded that this difference was simply caused by the difference between the simulations idealities and the inevitable real world non-idealities.

Measurements continued by adding the model space suit. Up to this point the antenna was tested in open space. First we looked at S_{11} with the arm inside our first order suit model, an aluminum duct (see figures 2.17-2.19). The table below contains the results from these tests.

Position in duct	R (Ω)	X (Ω)	Frequency
1/3 from top	24.9	-34.5	315 MHz
1/3 from bottom	43.8	-39.6	315 MHz
center	64.6	-32.1	333 MHz

Table 2.6 S_{11} in Aluminum Duct at Three Positions

Unfortunately since the center of duct measurement was taken at a different frequency it is hard to compare it directly to the other values. The following images show the Smith Chart

from 300 kHz to 3 GHz and thus are more reasonable to compare. All three measurements show similar trends, but magnitude of S_{11} changes. Generally, the magnitude is lowest for one third from bottom while the other two are more similar. As expected, all three conditions result in a capacitive load at lower frequencies and an inductive load at higher frequencies; however, at the highest frequencies the load returns to being capacitive. As the frequency increases, the wavelength decreases and thus the top hat antennas size relative to wavelength increases. Since the primary concern in this project is the use of the lower frequencies (around 400 MHz) these results are not critical.

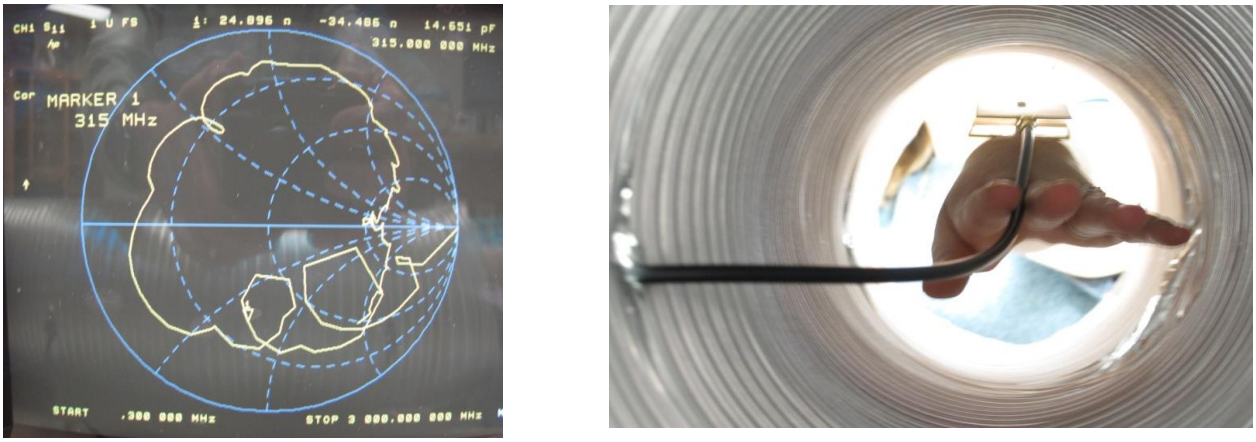

Figure 2.17 S_{11} in Aluminum Duct with Antenna One Third below the Top

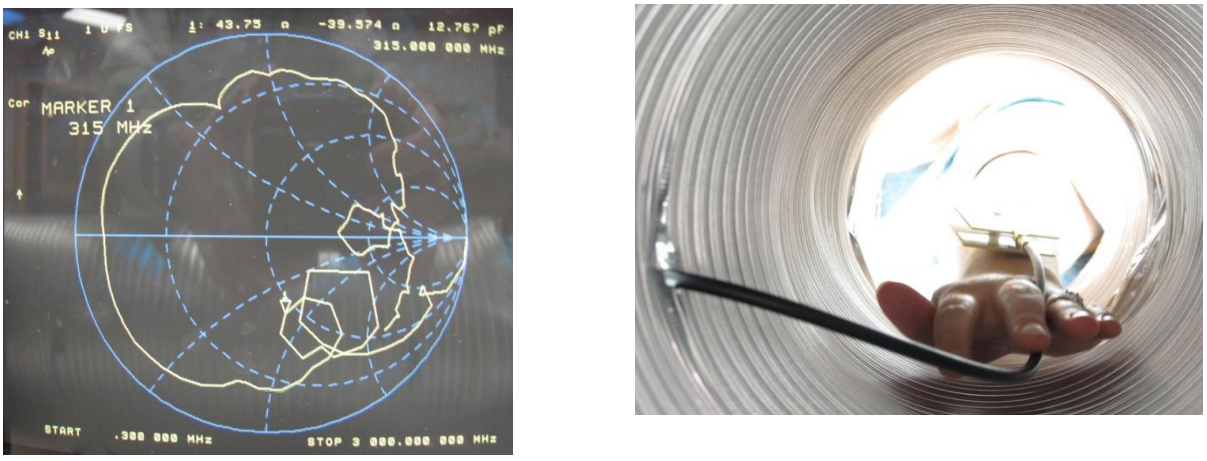

Figure 2.18 S_{11} in Aluminum Duct with Antenna One Third above the Bottom

Figure 2.19 S_{11} in Aluminum Duct with Antenna Centered

It is interesting to note, around 315 MHz there is a loop in the Smith Chart indicated a resonance with a large change in both resistance and reactance. This loop also indicated that a slight variation in frequency can drastically change the required matching network. The variation with the arms position relative to the tube will make it difficult to get a perfect match, but an imperfect match may provide significant increase to the signals strength.

2.3.2 Problems in Antenna Measurements

After taking these measurements we concluded that the benefits of a matching network would be minimal, since the antenna seemed fairly well matched and S_{11} varied widely depending on the arm's position. As we thought a little more critically about why the measurements did not match simulations, we realized the error. The concept of ground was misleading. Any good electrical engineer knows that ground is a reference point and therefor can be anywhere. In our top hat antenna the large metal flood, representing the ground plane of the radio, was assumed to be the ground. Looking at the entire system, inclusive of the human body, it is easy to see that the human body becomes the ground. In addition the cable from the network analyzer increased the physical size of the antenna. Our measurements were invalid. Section 3.2.2 explains this issue in more detail. To fix this error we needed to invert the antenna. This reduces the effect of the coax cable.

2.3.3 Correcting Initial Measurements

A new set of measurements was taken with the ground of the coax touching the arm (figure 2.20-22). Besides this orientation modification, the set-up is the same as before. All were done in the same environment with the antenna in free space, on the arm, and on an arm shaped ground plane. Table 2.7 shows these results. Compared to the incorrect measurements there is a decrease in resistance while reactance is similar. It is worth noting that the resistances and reactance are clustered closer together for the corrected measurements regardless of test conditions. These measurements are much closer to the simulated behavior and are believed to be more faithful to the actual impedance that will be seen by the battery powered radio with no coax cable to distort the fields.

Test condition	R (Ω)	X (Ω)
on gnd plane	1.0	-45.1
on arm	2.6	-44.5
on arm gnd	2.3	-43.3

Table 2.7 S_{11} at 433 MHz under Three Test Conditions

Figure 2.20 Top Hat Antenna on Ground Plane

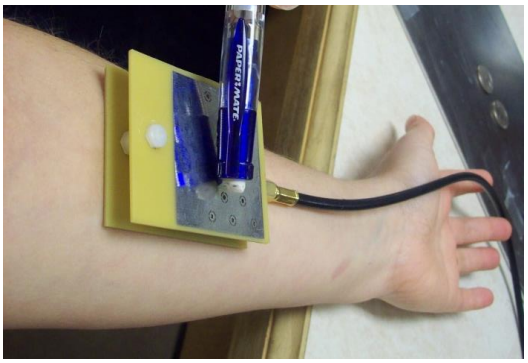

Figure 2.21 Top Hat Antenna on Arm

Figure 2.22 Top Hat Antenna on Arm Shaped Ground Plane

The simulations were done with an infinite ground plane. In simulation the resistance is smaller than measured, most likely resulting from ideal metals. Capacitance is also smaller in simulations. This may be the result of non-ideal materials.

Momentum		FEM	
R (Ω)	X (Ω)	R (Ω)	X (Ω)
0.13	-41.98	0.78	-30.65

Table 2.8 S_{11} From Simulations at 433 MHz

2.3.4 Conclusions on Matching Networks

From the previous measurements it is clear that matching will be a difficult task. To better understand the effects of an L matching network we tested the antenna under three different scenarios: no match, match, and imperfect match. S_{11} measurements were taken using an Hewlett Packard 8753E Network Analyzer. The antenna was in free space, no on-arm measurements were taken. Figure 2.23 shows the test set up. Table 2.9 shows the compiled data. When the top hat antenna is unmatched it exhibits equally low return loss over a wide range of frequencies. It is the matching network that determines the frequency of operations. Figures 2.24-2.26 provide a visualization of the data from 30 kHz to 1 GHz.

Type of Match	Frequency	S_{11} (dB)
No Match	400.0 MHz	-0.28
Match	405.3 MHz	-7.03
Imperfect Match	405.3 MHz	-1.36

Table 2.9 S_{11} for Three Different Matches

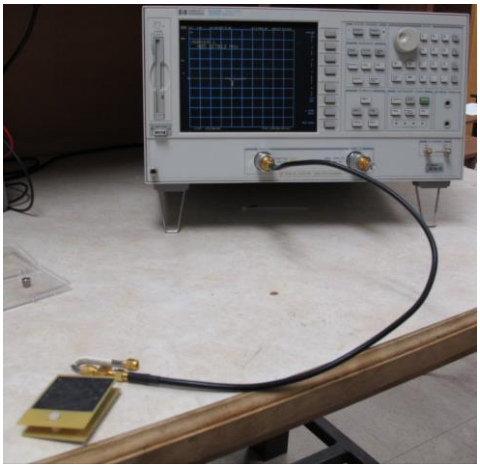

Figure 2.23 Setup for S_{11} Measurements (shown with match)

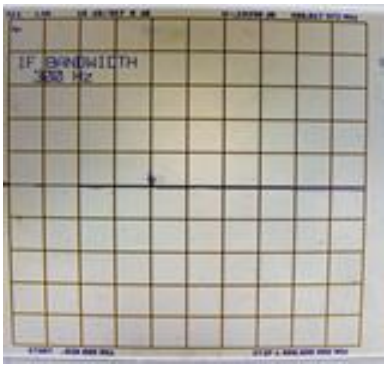

Figure 2.24 S_{11} Unmatched

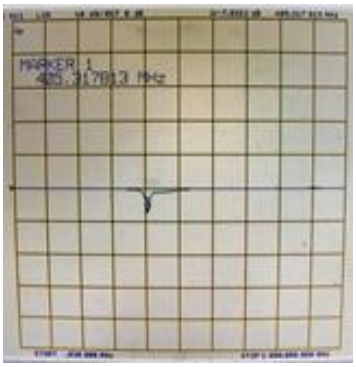

Figure 2.25 S_{11} Matched

Figure 2.26 S_{11} Imperfect Match

These tests illustrate that an imperfect match is better than no match. The closer the match is to perfect, the less the loss. This conclusion is further supported by field strength measurements. Figure 2.27 shows the top hat as the transmitter antenna, and a short dipole antenna functioning as the receiver antenna. The receiver antenna is connected to a spectrum analyzer while the transmitter antenna is driven from the network analyzer. Figure 2.28 shows the matched response laid over the unmatched output. The matched response is bold while the unmatched is faint. The received signal appears to be approximately 10 dB stronger even with the imperfect match.

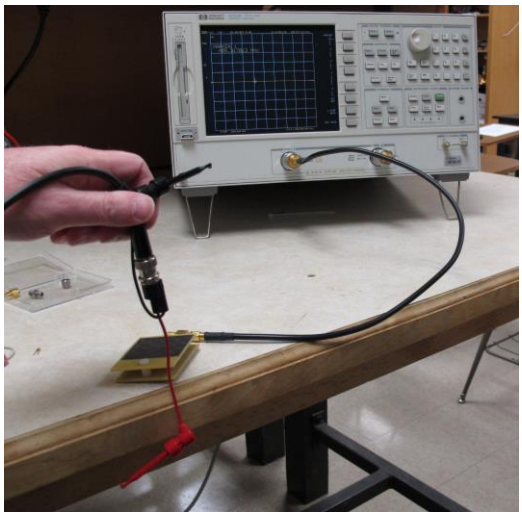

Figure 2.27 Measuring Field Strength

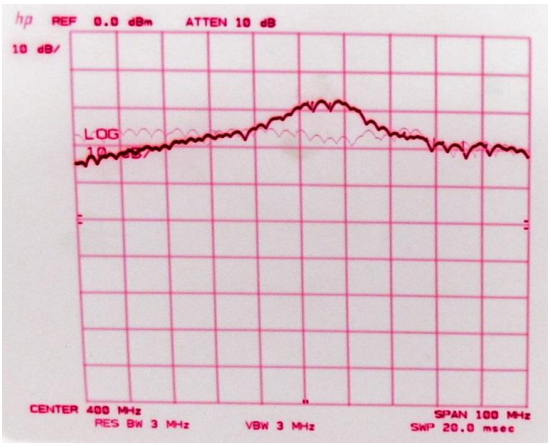

Figure 2.28 Received Field Strength

From these tests it is clear that a matching network should be implemented. Even an imperfect match will provide substantial gain. It is also important to note that the 10 dB gain is representative of only the transmitter being matched. If both transmitter and receiver are matched the gain relative to use with an unmatched top hat antenna would be closer to 20 dB.

Ideally, the antenna's return loss would be measured while being worn inside the suit by the astronaut who will use it. A first order approximation can be made using our model suit and a willing researcher. Designing and implementing the matching network is left as future work.

Chapter 3 - Testing the Antenna in Space Suit Models

3.1 Physical Models of the Spacesuit

3.1.1 The Need for a Physical Model

The spacesuit presents a unique radio environment. Multiple layers of aluminized mylar are part of the thermal-micrometeorite garment that makes up the outermost layer of the suit. These layers protect the astronaut from extreme temperatures and micrometeorite, as the name implies; however, the aluminized mylar also has strong implication to radio signals [16]. Depending on thickness, aluminized mylar may be opaque to radio waves, thus making an astronaut's body area network different from current understanding of body area networks. After testing a sample stack up sent by ILC Dover, the team was able to confirm that the aluminized mylar is radio opaque at 400 MHz and above.

3.1.2 The Models

To test and refine an antenna designed for use inside a spacesuit and ultimately to measure the radio signal path loss between a transmitter and receiver inside the suit, it is important to understand the space suit environment. Since it is difficult and expensive to conduct testing with a real spacesuit, the research team came up with two different physical models [17]. For a first small scale model we used a flexible duct similar to one used for venting a dryer. The flexible duct is about three times the diameter of the arm and may be larger than the actual suit but provided a first look at the radio environment. Since the duct is made of aluminum its conductive characteristics is comparable with the real suit. This model was only used for small scale testing. In the previous chapter some of the S_{11} measurements were taken inside the duct. As shown in section 2.3.1, S_{11} changes when the arm is placed inside the duct. Furthermore, it varies as the antennas position relative to the duct changes.

The second physical model is a full scale model. It contains a layer of copper fabric in place of the aluminized mylar of a real suit. After evaluating the electrical properties of many conductive fabrics the team determined that the copper fabric would be the best choice. Erin Monfort-Nelson, a graduate student in Apparel, Textiles, and Interior Design, designed and constructed a space suit using the metallic fabric. The suit was modeled from the Extravehicular

Mobility Unit (EMU). The figure below shows the full suit with patches added to give a more authentic appearance.

Figure 3.1 Full Scale Model with Prop Helmet and Boots

Pieces of this full scale model can also be used as a small scale model. Before taking full suit measurements a few small scale measurements were made with the sleeve being used in place of the duct.

3.2 Testing in Full Scale Model Suit

3.2.1 Initial Pre-suit Test

Before the model suit was ready, we wanted to examine the testing method. The original plan was to use a car key fob and the top hat antenna discussed in the previous chapter. The key fob was the transmitter and wired to be on continuously. The top hat antenna connected by coaxial cable to a spectrum analyzer was the receiver. By connecting the top hat antenna to the spectrum analyzer we could measure the received power. For all test the key fob transmitter was placed on the back of the neck (figure 3.2). The test results are shown below in table 3.1.

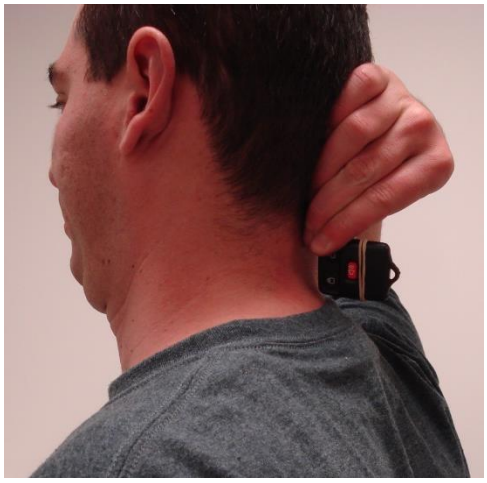

Figure 3.2 Location of Key Fob Transmitter

RX Antenna Location	RX Power (dBm)
ankle	-50
wrist	-49
mid-calf	-42
mid-lower arm	-42
mid-upper arm	-40

Table 3.1 Received Power at Various Locations on the Body

After comparing the received power at various locations we could draw a conclusion about the path loss. Since these initial tests were done in a lab known for having significant multipath, the data is skewed, but it was a way to check our preliminary thinking. This data was not analyzed in depth due to conclusion drawn later in the same day. It seemed a little strange that the ankle and wrist would have the same received power, as well as mid-calf and mid-lower arm. The next section outlines the issue.

3.2.2 Coupling Issues

At higher frequencies, the component's functions change due to complex electromagnetic field interactions, especially in the case of antennas. For example wires, even with shielding, can become antennas—since the simplest antenna is a wire.

3.2.2.1 A First Look at the Coupling Issue

In the test set up, the long coax cable connected to the spectrum analyzer was behaving as an antenna. The transmitted signal is coupling onto the coax cable and thus the receiver antenna size was much larger than it would be in practice.

antenna connection to spectrum analyzer	transmitters orientation	TX to RX distance order of magnitude	Power (dBm)
direct	copolar	cm	-38
direct	crosspolar	cm	-45
long cable	next to cable	m	-20

Table 3.2 Received Signal Strength

Direct Connection vs Long Cable Connection

Table 3.2 shows the power received by the top hat antenna. The first two entries have the antenna directly connected to the spectrum analyzer. The transmitter is centimeters from the top hat. The copole orientation should provide the strongest signal and the crosspole the weakest. However, when the antenna is attached with a long cable the receive signal is stronger. The transmitter orientation remains copolar and the distance between the transmitter and receiver is increased. These changes should result in a weaker signal. The only way the signal could be stronger is by coupling into the cable. That is the cable becomes part of the receive antenna.

This coupling is an undesired effect. Received signal strength is falsely reported. The longer the cable the greater the amplification as the wire becomes an antenna itself. One known way to mitigate this effect is the use of a radio frequency choke. The choke should reduce the magnitude of the coupled signal. In this case, since the interfering frequency is the same as the desired frequency, a choke is an ineffective strategy. Figures 3.3and 3.4 show the resulting change to be around 1 dB. The left image is of the baseline image while the right image has the RF choke implemented.

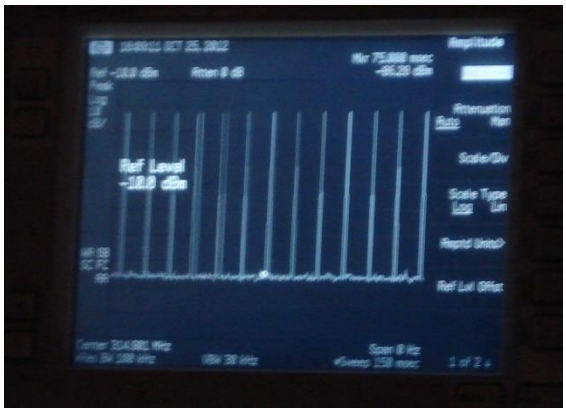

Figure 3.3 Cable without Choke

Figure 3.4 Cable with Choke

The choke does not eliminate nor drastically reduce the cable coupling thus a better solution was required. Ideally the cable would be eliminated and measurements made wirelessly. This is the main motivation behind the wireless measurement methodology ultimately adopted in section 3.2.3.

3.2.2.2 A Second Look at the Coupling Issue

Looking at S_{11} and the antenna's placement on the arm we also see the effects of coupling. The following series of photographs were taken during measurement of the antenna. It is clear that the coax cable will couple with the signal.

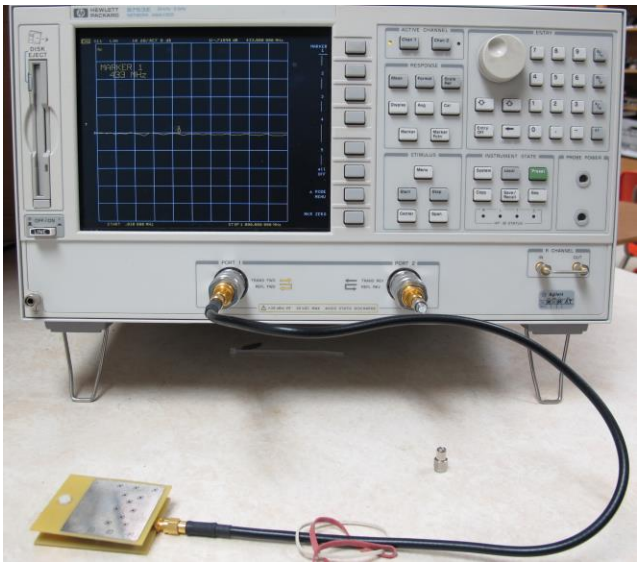

Figure 3.5 S_{11} for Antenna off Arm

Figure 3.5 illustrates the antenna S_{11} response when it is not on the arm. The on-arm response should be similar to the off-arm response; however, the on-arm response in figure 3.6 shows a dramatically different S_{11} due to the top hat coupling to the coax cable. Here, the arm becomes one side of a dipole and couples to the coax, which acts as another dipole element. This results in a physically larger structure with artificially improved return loss.

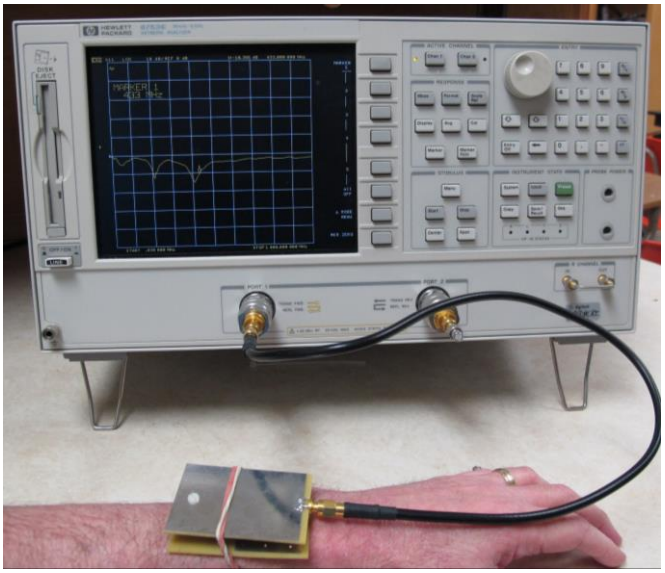

Figure 3.6 S_{11} for Antenna with Top Hat on Arm (Inverted Top Hat)

Figure 3.7 shows a measurement which is more faithful to the actual operating conditions. The coupling is reduced due to having the coaxial cable touch the arm and providing a shorter path to ground.

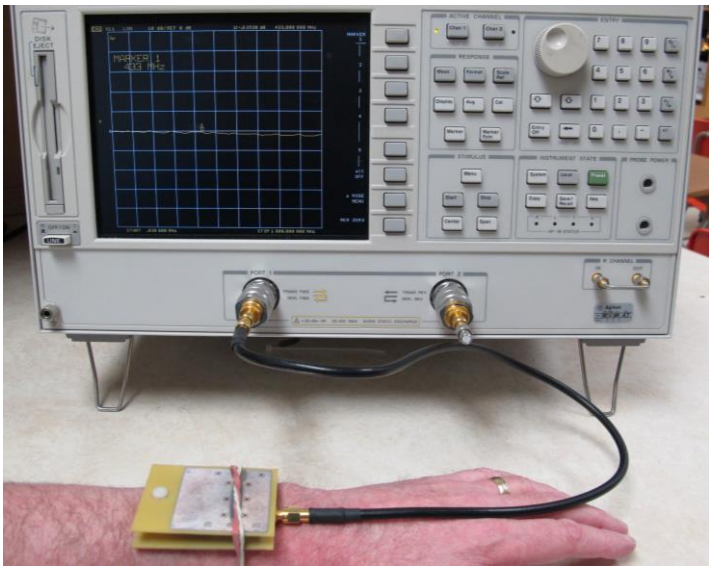

Figure 3.7 S_{11} for Antenna with Ground Plane on Arm

This indicates coupling can be a major issue for antenna measurement. Further studies should be conducted on this issue. The next section discusses the wireless option as well as the issue of intra-suit testing.

3.2.3 Solution to Coupling and Intra-Suit Measurement Problems

Making wireless measurments appeared to be the most feasible option for solving the coupling issue. The team was able to purchase a commercial radio board from Parallex [18] with a received signal strength indicator (RSSI) output. Furthermore, the boards transmitted at 0 dBm signal strength. Therefor the received signal power is equal to the pathloss. Figure 3.8 shows the input and output interface. The monopole antenna is easily removed and the top hat attached. This radio provided a simple and compact solution to the coupling issue; however, the question of how to get the received signal strength information outside of the suit remained a problem.

Figure 3.8 Radio Inputs and Outputs Interface

The RSSI line can be utilized in many ways. The simplest solution would be to attaching a digital multimeter or an oscilloscope and read of the analog voltage, but that adds wires to the system. Another option would be programming a microcontroller to convert the RSSI voltage to the equivalent power and send it to an LCD. Again, within the spacesuit this is not an option since the displayed data cannot be seen. A similar, but more feasible option would be having the microcontroller store the data. Then, after the test is over, the data could be extracted. From previous experience, I was not inclined to use a microcontroller. Programming would take too much time and the delay in extracting the results prevents making real time observations that can be very useful in a preliminary investigation.

The option selected was adding an audio oscillator which has its frequency controlled by the analog RSSI voltage. The audio signal could be transmitted through the suit because of its

acoustic behavior. Furthermore the audio oscillator is a simple circuit which can be built quickly from components readily available in the Electrical and Computer Engineering Student Shop.

3.2.4 Implementing an Audio Oscillator

There are three major constraints on this audio oscillator: (1) its input voltage range must span 0.4 V to 1.6 V to cover the range of the RSSI output, (2) it must run on a 3.7 V lithium ion battery, and (3) it must output a frequency in the middle of the audio range. Based on readily available parts, the 555 timer was selected to be the active component in the audio oscillator. The 555 timer was used in astable operation. According to the datasheet for a supply voltage of 1.5 V the control voltage should be 0.8 - 1.2 V and for a supply voltage of 5V the control voltage should be 2.9 - 3.8 V. The supplied voltage in this system will be between these two values, thus the upper values should be at least 1.6 V. The lower range values was of concern, but after building the circuit, it was found that the lower power value was enough to cause the desired oscillation frequency control. The use of a 0.5 ms time constant would produce a 1.5 kHz nominal pitch which is well within the audio range.

The oscillator was built using the same resister values as in the datasheet. The capacitor value was chosen based on the 0.5 ms time constant. In addition to the audio oscillator circuitry, a low pass filter was added between the radio's RSSI output and the control voltage of the 555 timer. The schematic is shown in the figure 3.9.

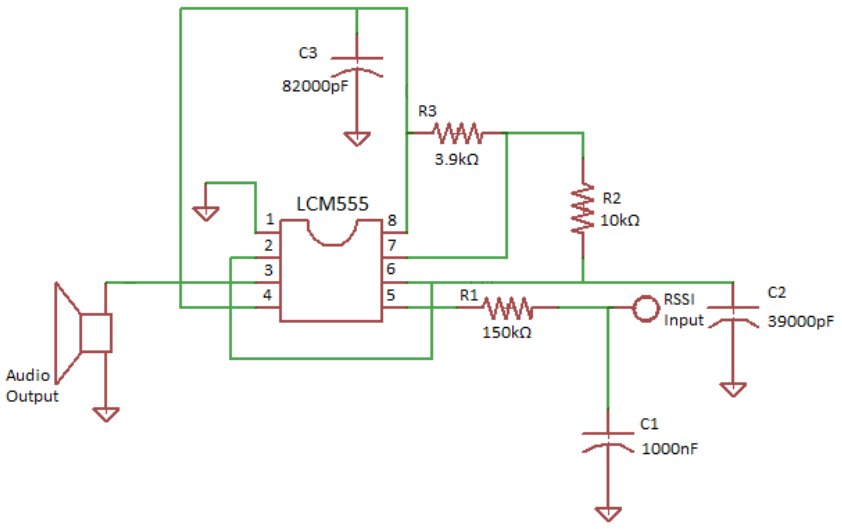

Figure 3.9 Audio Oscillator Schematic

3.2.4.1 Received Power to Audio Frequency Mapping

Before the audio oscillator could be used, a conversion graph needed to be created. To create a conversion graph we mapped received power to the output frequency. A radio frequency signal generator was connected to the antenna port of the radio board. The audio oscillator circuit was connected to the radio's IO interface and a power supply or lithium ion battery was used to power both radio and oscillator. To quantitatively evaluate the frequency a directional microphone was connected to an audio amplifier with its output fed to an oscilloscope (figure 3.10). The math function on the oscilloscope was used to perform a Fast Fourier Transform (FFT), thus providing a quicker and more accurate frequency measurement.

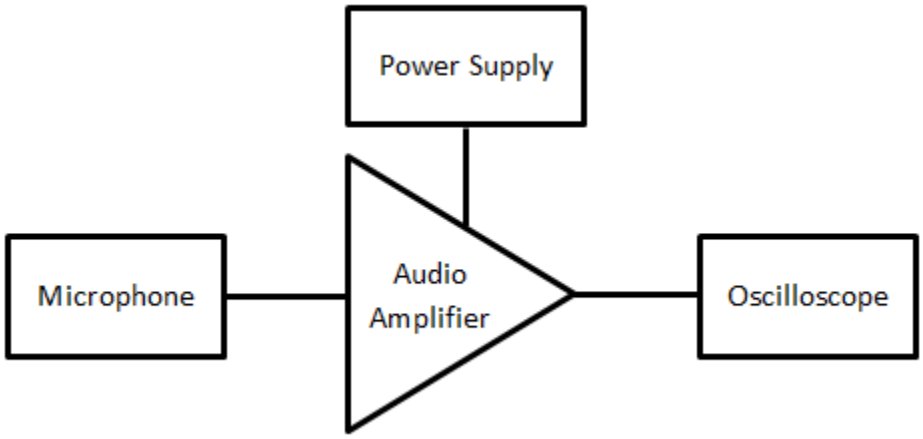

Figure 3.10 Test Setup Block Diagram

The RF signal generator was set to 433.42 MHz frequency and -30 dBm power. Based on the RSSI curve in the radio chips datasheet [19] the RSSI voltage levels off at power levels greater than -35 dBm and at power levels lower than -115 dBm. The power was stepped down in 10 dB or 5 dB increments, depending on the test date. Multiple measurements were taken. Most involved a change in supply voltage either by changing the voltage on the power supply or the draining of the battery over time. Figure 3.11 represents the mappings for three different tests. They are labeled by the date taken. Measurements on 11 Dec were done after a set of in-suit measurements. Measurements on 12 Dec were done after a series of measurements in the suit. The up and down labels refer to the test being conducted for higher power to lower power (down) or from lower power to higher power (up). The tests were done consecutively.

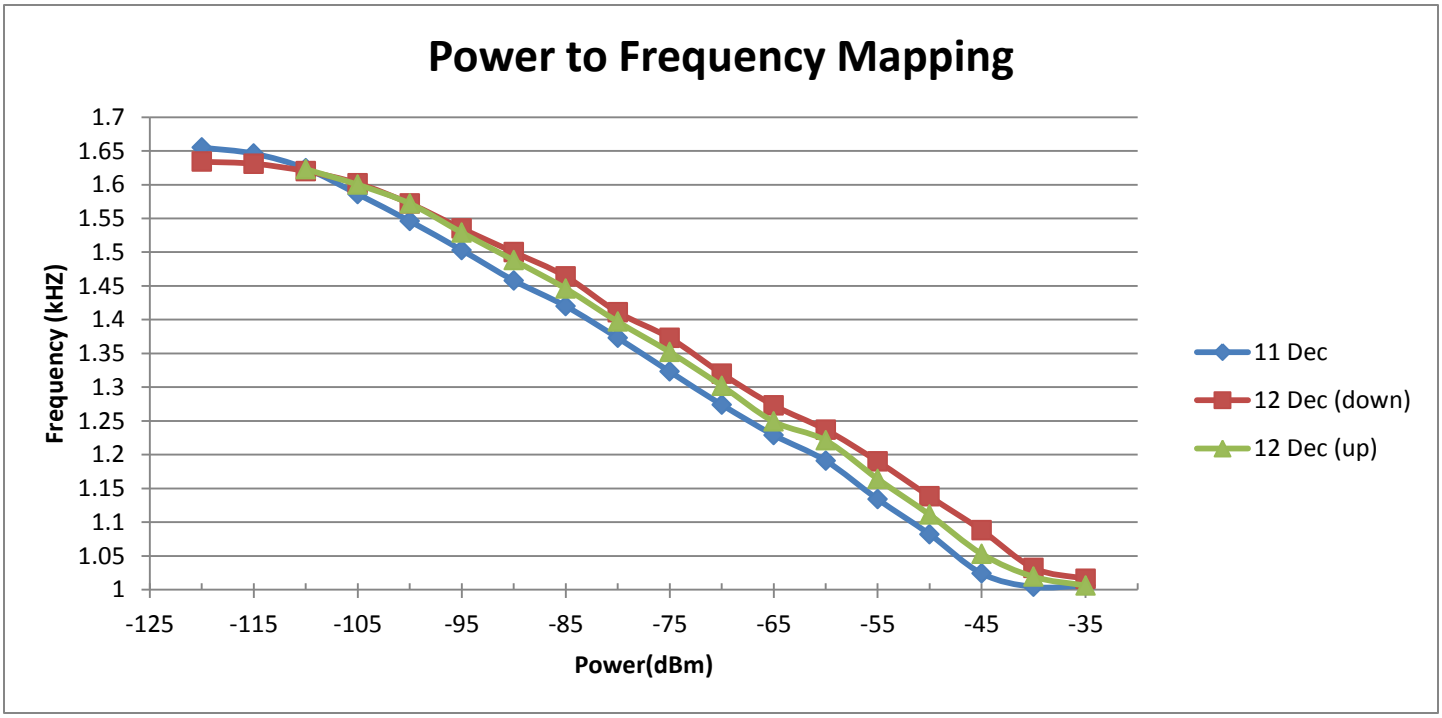

Figure 3.11 Sample Set of Power to Frequency Mapping

This data lead us to believe a matching network might be hazardous to testing. The radio transmits a 0 dBm signal. If the matched antennas are placed in close proximity the received power could be greater than the -35 dBm sensitivity. The information would be interpreted to represent the -35 dBm signal when it might actually be stronger. To prevent this misrepresentation of received power the matching networks were excluded from both antennas. With the addition of the matching network, the mismatch loss was found to be improved by 20 dB. By omitting of matching, signals as strong as -10dBm could be received.

3.2.5 In-Suit Test Set Up

The in-suit test set up requires the same equipment mentioned in the previous section (figure 3.10). By using the calibrated graphs (figure 3.11) the frequency can be translated to power received. Based on the calibration graph there was a limited range of frequencies from around 1 kHz to 1.7 kHz. The span of the oscilloscopes' FFT function was set to 2 kHz and centered at the nominal frequency of 1.5 kHz. This limited the second harmonics which could be seen. Furthermore, if any signal was above 1.7 kHz it had to be a second harmonic and another peak (often weaker) could be found at half the frequency of the second harmonic.

Initial testing was completed using only the mitten, arm, and torso of the suit. These measurements were taken with both radios on the arm and using 15 cm, 30 cm, and 45 cm distance between the transmitter and receiver. This set of data would be compared with electromagnetic simulations [17]. The primary purpose of later tests was to determine the feasibility of using the antenna for an in-suit network. The figure below shows the antenna locations. Table 3.4 refers to these locations.

Location		Color Code
TX	RX	
wrist	arm cm measurements	Green
R Leg	L Leg	Orange
L wrist	R wrist	Red
L wrist	L ankle	Purple
ankle	leg cm measurements	Blue
chest	shoulder	Black
chest	mid upper arm	Black
chest	mid lower arm	Black
chest	mid calf	Black

Table 3.3 Radio Location Reference

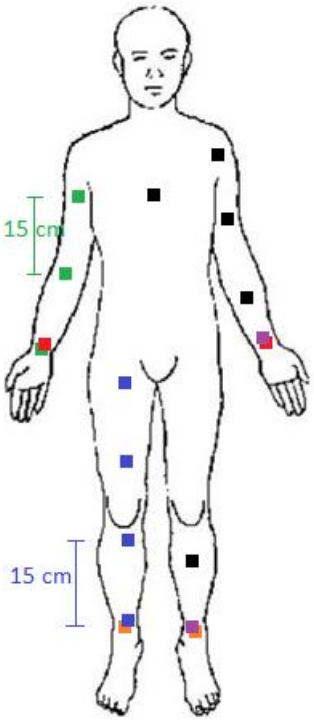

Figure 3.12 Radio Locations

These locations were selected after consulting with task one researchers. Many of the locations are current sensor locations in their testing. Since the radio will be implemented in conjunction with the sensors it seemed reasonable to use potential sensor locations to evaluate radio transmission. However, since the sensors locations are relative positions, the distance between sensors will vary from person to person.

For testing, the top hats were placed directly on the skin as shown in figure 3.13. Initially rubber bands were used to hold the radios and antennas in place with bubble wrap used to separate the antenna from the suit (functioning as the air gap). Later on, Velcro straps were used to fasten the radios and antennas with two layers of sweatpants and sweatshirts used to prevent

contact with the suit (bubble wrap was used on the hands and around the neck). The following figures are a collection of test photos to help understand test set up, and they are followed by a more detailed explanation.

Figure 3.13 Measuring Radio Spacing shown at 15 cm moving to 30 cm

Figure 3.14 Using Bubble Wrap for Air Gap

Figure 3.15 Reviewing Radio Locations

Figure 3.16 Placing Antenna on the Arm

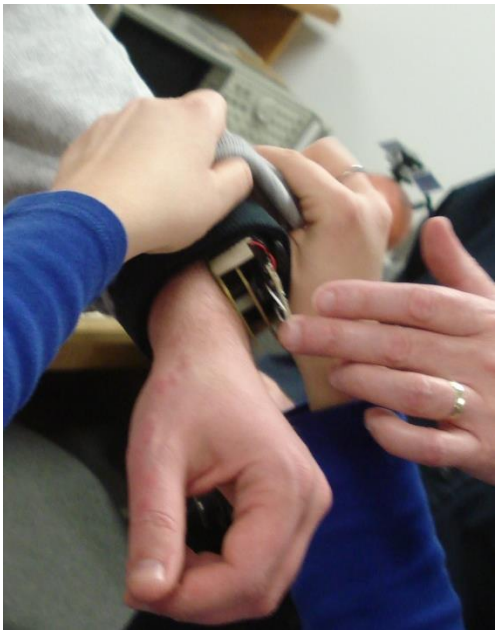

Figure 3.17 Using Sweatshirts to Represent Air Gap

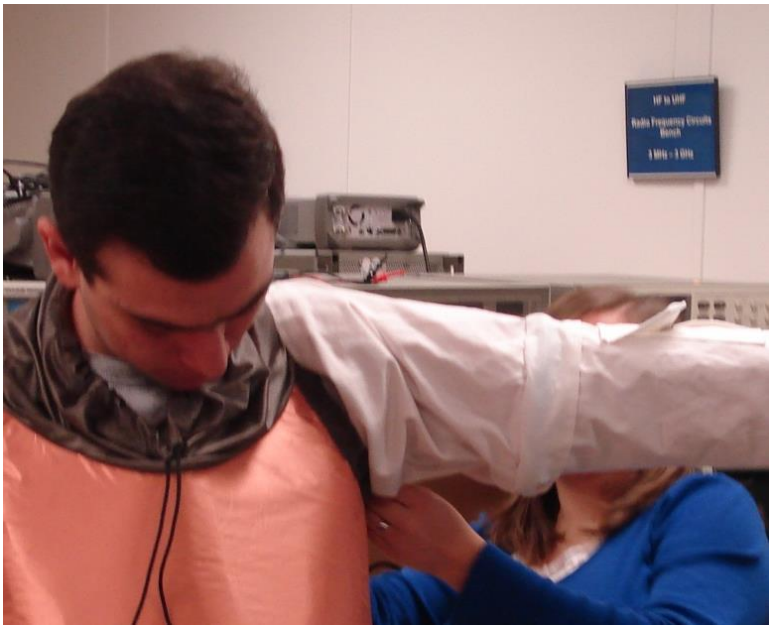

Figure 3.18 Attaching the Arm of the Model Space Suit

Figure 3.19 Placing Antenna on Leg

Figure 3.20 Close up of Antenna, Radio, and Audio Oscillator on Leg

Figure 3.21 Attaching Leg of the Model Space Suit

The first two images show the initial test set up using bubble wrap. The paper seen in figure 3.13 is marked at 15 cm. These measurements were taken to be compared with electromagnetic simulations [17]. As evident in the photo these measurement were not taken in the full suit. The rest of the measurements used the full suit. Figures 3.16 and 3.17 show the antenna's placement on the arm and the two layers of sweatshirt used to establish a gap. Similarly, figures 3.19 and 3.20 show the placement on the leg. Regardless of location, the antenna is positioned with the top hat directly on the skin.

Other relevant information includes how to put the spacesuit together. Figure 3.18 shows the Velcro attachment of the arm to the torso and figure 3.21 shows the lower leg component being attached with an embroidery hoop. The Velcro fastening should be familiar to most readers. In this case the Velcro material is a special conductive type to maintain electrical conductivity through the suit model. Unless the reader does embroidery it is unlikely she/he is familiar with an embroidery hoop. The concept is based on two circular hoops with one slightly smaller than the other. The larger hoop has an opening and is fastened together using threading and a nut—thus allowing for different thicknesses of fabric. In the spacesuit the lower leg component is the smaller hoop, the larger hoop is built into the shorts. To secure the lower leg section, place the smaller hoop inside the larger hoop and tighten the nut. The small hoop should be concentric with the larger one. The copper fabric of the smaller hoop should contact that of the larger hoop.

Other suit joints are the torso to the shorts. This is a simple conductive Velcro connection. The arms to the mittens are electrically connected with the overlap of the conductive stretch fabric. The same technique is used for the legs and feet.

3.2.6 In-Suit Test Findings

Multiple mappings were used to convert the frequency to received power. Since the transmitted power level is zero the magnitude of the received power is the path loss. In these cases the raw data in table 3.4 includes both the path loss and mismatch loss. With the addition of a matching network the received signal would be stronger and the path loss less. The table on the next page is organized by the date of the test. Six different mapping (discussed in section 3.2.4) are used—also organized by date. From the mapping three averages are taken (shown in blue, over three mapping, and in green, over all mapping). Averaging helps account for human

errors that may have occurred when creating the mappings or reading values off the graphs. The table also provides some insight on the test conditions and the radios' locations.

			Mapping date	16 Nov (dBm)	6 Dec (dBm)	11 Dec (dBm) low	Average of first three	11 Dec (dBm) high	12 Dec (down) (dBm)	12 Dec (up) (dBm)	Average of last three	Average of all values	Notes about testing
results by dates				values approximated based on frequency mapping									
6-Dec	frequency												bubble wrap only torso, one arm and mitten of suit
15 cm on arm	1.165 kHz			NA	-53	-57.5	-55.3	-57.6	-52.5	-55	-55	-55.1	
45 cm on arm	1.252 kHz			NA	-59	-68	-63.5	-67.5	-62	-65	-64.8	-64.3	
11-Dec	frequency	fundamental											with skin contact at neck and two layers of sweatshirts
R leg to L leg	2.23 kHz	1.115 kHz		NA	-48	-53.5	-50.8	-53	-48	-50	-50.3	-50.5	
L arm to R arm	1.54 kHz	1.54 kHz		-66	-80.5	-87	-77.8	-99.5	-95	-96	-96.8	-87.3	
12-Dec	frequency	fundamental											two layers of sweatshirts and bubble wrap on hands and neck
antennas at L and R wrists													
arms spread straight out	1.435 kHz	1.435 kHz		-65.5	-81	-87	-77.8	-87.5	-82.3	-84	-84.6	-81.2	
arms by side	1.518 kHz	1.518 kHz		-77	-90.5	-96	-87.8	-96	-92	-93	-93.7	-90.8	
one arm in front one behind	1.447 kHz	1.447 kHz		-67.5	-83	-89.5	-80	-89	-83	-85	-85.7	-82.8	
RX bent 90 TX straight out	1.499 kHz	1.499 kHz		-74.5	-88.5	-95	-86	-94.5	-89.5	-91	-91.7	-88.8	
TX up (Statue of Liberty)RX at side	1.433 kHz	1.433 kHz		-63	-80.5	-87.5	-77	-86.5	-82	-83.5	-84	-80.5	
TX in front (holding juice) RX at side	1.518 kHz	1.518 kHz		-76	-90	-97	-87.7	-96.5	-92.5	-93.5	-94.2	-90.9	
wrists and ankel (same side)													
arm straight out standing	1.642 kHz	1.642 kHz		-94	NA	-118	-106	-113	NA	NA	-113	-108	
arm at side standing	1.597 kHz	1.597 kHz		-87	-100	-106	-97.7	-107	-103	-104	-105	-101	
sitting arm at side	1.597 kHz	1.597 kHz		-87	-100	-106	-97.7	-107	-103	-104	-105	-101	
sitting arm crossed at lap	1.654 kHz	1.654 kHz		-95	NA	-117	-106	-118	NA	NA	-118	-110	
10-Jan	frequency	fundamental											two layers of sweatshirts and bubble wrap on hands and neck
30 cm on leg	2.037 kHz	1.0185 kHz		NA	NA	-45.5	-45.5	-44.5	-38	-40.3	-40.9	-42.1	
45 cm on leg	2.275 kHz	1.1375 kHz		NA	-59	-54.5	-56.8	-55	-50	-52	-52.3	-54.1	
14-Jan	frequency	fundamental											two layers of sweatshirs and bubble wrap and hands and neck
TX on chest													
RX at shoulder	2.393 kHz	1.197 kHz		NA	-55	-60.5	-57.8	-60.5	-55.5	-57.6	-57.9	-57.8	
RX at mid upper arm	1.278 kHz	1.278 kHz		-41	-62	-71	-58	-69.6	-65	-67	-67.2	-62.6	
RX at mid lower arm	1.311 kHz	1.311 kHz		-49	-68	-74.7	-63.9	-74	-69.3	-71	-71.4	-67.7	
RX at mid calf	1.459 kHz	1.459 kHz		-66.7	-83	-89.5	-79.7	-90.3	-84.6	-86.6	-87.2	-83.5	

Table 3.4 Antenna Test Data

When collecting the data, researchers found that the second harmonic was often stronger than the fundamental. This is noted in the table by the two frequencies. The first is the frequency read off the oscilloscope while the second is the fundamental. Initially when the frequency was outside of the mapping range it was assumed to be the second harmonic.

However, if the fundamental was also outside of the range then it was concluded that the frequency indicated a system error.

From the data presented in table 3.4 we can draw a few simple conclusions. First, traveling through the chest cavity results in a large loss. Further research is necessary to determine the exact cause of this increased loss. One possible explanation is the torso section acting as a resonate cavity. Future work will be conducted in the suit with radios at different frequencies. If these effects seem to be reduced at other frequencies, the resonance becomes a more probable cause. A second explanation is the possible pinching off of the gap between the arm and the suit. In this case the loss should be fairly consistent across a range of frequencies. Second, a radio placed on the chest or back should be able to receive data from another radio anywhere on the body. This is true even with the large loss in the chest cavity as this loss is reduced when one end of the radio communication is on the chest or back. Furthermore, current suit design has a hard wired link out of the suit to the backpack. This existing link could be used with a central radio, on chest or back, to transmit the data outside of the suit.

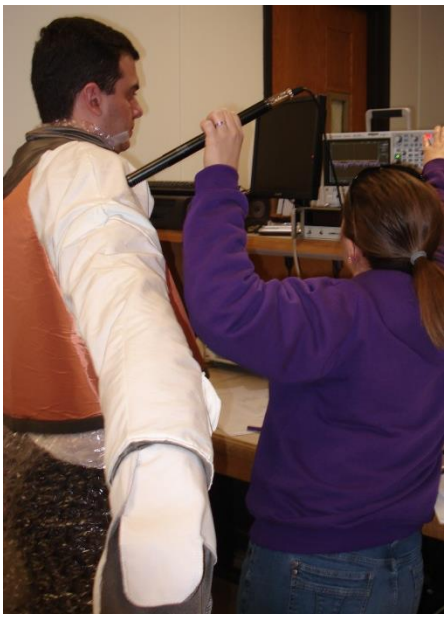

Figure 3.22 Early Experiments Measuring Frequency

Figure 3.23 Measuring Frequency Full Scale Test

Chapter 4 - Exploring Energy Harvesting

4.1 Background Study of Energy Harvesting

4.1.1 What is Energy Harvesting

Simply put, energy harvesting is converting already available energy to a more useful form. Often the energy being harvested is considered wasted; sometimes it is a byproduct of another energy conversion (i.e. heat off electrical components). One of the most well-known forms of energy harvesting is photovoltaic cells. Most elementary school students are familiar with solar calculators. These calculators contain photovoltaic cells which convert light to electrical energy. In a low power system, like the calculator, the term energy harvesting is use. When the same concept is applied to a high power system, like a solar cell farm, the term alternative energy is used.

Name	**Concept**	**Benefits**	**Drawbacks**
Nantennas or Antennas	RF at one or more frequencies converted to electrical energy	Commonly used (RFID tags) [21]	No RF radiation in the spacesuit
Piezoelectric	Mechanical energy (pressure, force and vibration) converted to electrical energy	Many piezoelectric materials [20]	Motion/force required
Photovoltaic	light converted to electrical energy	Well understood	No light in the spacesuit Low efficiency
Pyroelectric	Time varying temperature converted to electrical energy		Time varying
Thermoelectric	temperature gradient converted to electrical energy	Temperature gradients ubiquitous	Low output voltage
Wind turbine	Wind spins turbine and converts mechanical energy to electrical energy	Well documented Well understood Fair efficiency	Minimal air motion in spacesuit large size

Table 4.1 Energy Harvesting Options

Since the power requirements for personal electronics are being reduced, energy harvesting is becoming more feasible and many researchers are exploring the various options. One researcher at ETH Zürich is interested in smart clothing and integrating power and data [20].

The table above lists some different forms of harvesting electrical energy. It also provides a brief explanation of how the system works and if it could be used inside a spacesuit. Some are appropriate for in-suit applications while others would be more beneficial in a different setup. Benefits and drawbacks of each type of harvesting are listed as relevant to in-suit applications.

4.1.2 Previous Energy Harvesting Work at K-State

In recent years Kansas State University has contributed to alternative energy through the Kansas Winds Application Center (WAC). This organization is educating electrical engineers on wind energy basics, and being an information source to others Kansas interested in wind energy. As part of this effort WAC runs the Wind for Schools program; small wind turbines are installed on the campus of K-12 schools for educational use [22]. As a department our focus in energy harvesting has primarily been providing kilowatts of power. This changed in 2009, with the creation of a low power energy harvesting radio board. This radio board contained four 5 cm^2 solar panels, from solar powered calculator. Using indoor lighting these panels supplied enough energy to support 433 MHz bursts with a 0.2 km minimum range [23]. These two areas are the foundation of the energy harvesting work in the Electrical and Computer Engineering Department. Both wind and solar have many terrestrial applications, but when transitioning to in-suit applications wind and solar energy cannot be used. The next section explores energy harvesting technologies for potential use in the spacesuit.

4.2 Selecting a Focus Area

4.2.1 Infeasible Options for Use in a Space Suit

Some of the options listed in table 4.1 will not be useful inside the spacesuit to power a wireless sensor. For example, the only way for solar energy to be inside the suit is through a hole. If there was a hole in the spacesuit there would be no need for a wireless sensor as the astronaut would have bigger problems than monitoring health signals. Other devices are not

good options due to their physical size. Even a scaled down wind turbine would not fit in the spacesuit and in suit air movement is minimal. Nantennas are another challenging option for in-suit use. Harvesting radio frequency energy implies the presence of strong radio waves. Any radio wave in the suit is used for communication between the sensors and would produce less energy then it uses. In the case of RFID tags, there is a small radio powered chip which usually communicates with a higher power system, plugged into the electrical grid. In addition, the time varying temperatures required for pyroelectric energy harvesting do not exist in the suit. While there is a slight variation to the body temperature I believes the gradient might be too small for pyroelectrics to operate. The goal for this energy harvesting system is to create the least amount of interference with the astronaut's regular activities.

4.2.2 Down Selecting Feasible Options to One Area

The remaining three energy harvesting options pass the initial check. Each seems capable of in-suit use. The piezoelectric and automatic watches work on similar concepts converting a mechanical force to electrical energy. In [24] the piezoelectric effect is found to produce around 1μW per step when placed in the shoe. It is unclear how much gravity affects this type of generation, but if the astronaut is on a spacewalk there is no surface to push against and create pressure. Similarly automatic watches require regular motion to produce power. An automatic watch converts kinetic energy to electrical power. As the arm wearing the watch moves the energy is used to power the watch. More research would be necessary to determine the amount of energy that could be harvested in this way during EVA activities.

Thermoelectric is the remaining option. According to [24] the human body can produce watts of energy from body heat. This energy could easily be harvested for use with any electronic device attached to the body. It is an ideal option for biomedical sensors with skin contact. Thermal energy harvesting makes use of the difference of temperature on two parallel sides of a device. The following sections explore thermal energy harvesting in depth as well as how it could be utilized in the spacesuit.

4.3 Thermal Energy Harvesting

4.3.1 Basic Concept

Thermal energy harvesting is based on the Seebeck effect. This effect states that a voltage will be established across two dissimilar conductors at different temperatures. German physicist Thomas Johann Seebeck is credited with discovering this phenomenon in 1821. Over ten years later, Jean Charles Athanase Peltier would discover that a temperature difference could be created across two dissimilar conductors when a voltage was applied across the conductors. These effects are thermodynamically reversible. Thus a Peltier device can be used as a thermal energy harvester.

The conversion of thermal energy to electrical energy transforms energy typically considered to be wasted into a more useful form. A thermal electric generator (TEG) will provide electrical energy when one side has a hot temperature and the other has a cold temperature. In [5] the authors describe the development of a TEG. In this research the goal was to evaluate and incorporate a commercially available device. Due to the law of conservation of energy it is expected that larger temperature difference would produce a higher voltage. In an ideal situation the hot side of the TEG would be at a very high temperature while the cold side would be at a very low temperature. In practice this is difficult to realize. The next section explains how a TEG might be used in a spacesuit.

4.3.2 A Concept for In-Suit Application

The spacesuit contains a unique thermal environment. Of course the largest temperature difference would be between the human skin and the exterior of the suit; however, this is not a feasible option as a hole in the suit would be needed for its function. From our team's understanding of the spacesuit, the most logical location to place a TEG is between the Liquid Cooling and Ventilation Garment (LCVG) and the surface of the skin. For testing this concept the LCVG is assumed to be roughly room temperature. The LCVG contains 300 feet of plastic tubing which circulates two quarts of cool water every minute [16]. The figures below show an Apollo era LCVG in the care of the Kansas Cosmosphere and a sample of the LCVG sent by ILC Dover. Since the LCVG acts as a personal HVAC system, it is assumed that the temperature should be similar to standard room temperatures (around 20°C - 25°C).

Figure 4.1 Liquid Cooling Garment for A7L Suits at Kansas Cosmosphere

Figure 4.2 Liquid Cooling Garment in Sample From ILC Dover used in Current Suits

Before venturing further we needed to understand the temperature of the human skin and what affects it. The human body is a complex system which dissipates around 100 Watts of heat using three main techniques: radiation, evaporation and conduction. The largest percentage of heat is radiated infrared heat rays, second is evaporation and third conduction [25]. In addition [6] found that the head, chest, and location near an artery maximized TEG's power output. While the placement of sensors is dependent on the desired signals it may be beneficial to consider the use of these locations. A third article looks at the heat generated by the human body as it relates

to metabolism and suggests the activity level may affect the heat released from the body [5]. Therefore, more active astronauts lead to more energy. In addition, the water in the LCVG may result in a greater temperature change [25].

4.3.3 Surveying Available Products

There is a wide array of thermoelectric generators available, but most are designed for larger temperature differentials (10's to 100's of degree variations). Skin temperature to room temperature differs on the order of 10° C or less. Many devices are not sensitive to this small variation and of those that are, the resulting power is very small. A company in Germany is working to produce small thermoelectric generators with moderate power production. I made email contact with them and got an initial response but the conversation ended with my reply. Another company, Perpetua, is working to make extremely thin flexible bands. These bands consist of five thermoelectric generators (each roughly the size of a thumbprint) capable of producing 100 mW max output power at 2.5V [26]. Unfortunately, these bands were not on the market until early 2013 and won't be available commercially for another couple of years [27]. The fact that multiple companies are looking into thermal energy harvesting further reinforces its validity and potential usefulness.

While TEG's for small temperature differences are currently not readily available, Peltier devices are. Since the Seebeck effect is the inverse of the Peltier effect it seemed logical that the device may be capable of functioning in this manner. The next section addresses this initial concept test.

4.3.4 Initial Functional Evaluation

The first tests were conducted on a Peltier device used by previous students. Initially the research team was unsure of the response a Peltier device would have if instead of applying a voltage to produce a temperature difference, a temperature difference was applied to produce a voltage. The data sheets of Peltier devices do not address this reversible process. Data must be inferred from the graphs or tests must be conducted.

To test the concept we used a large metal plate at room temperature and an arm. The metal plate was placed on a desk. The cold side of the Peltier device was placed on the metal plate. The arm made contact with the hot side of Peltier device. The digital multimeter was

connected to the two wires. The short circuit current, the open circuit voltage, and the calculated output power—assuming an ideal fill factor of one—are shown in the table below. This data set represents only one person. Since the skin temperature varies from person to person the resulting voltage and current should also vary.

Open Circuit Voltage	50 mV
Short Circuit Current	7 mA
Output Power	350 µW

Table 4.2 Initial CP20151 Peltier Device Energy Harvesting Output

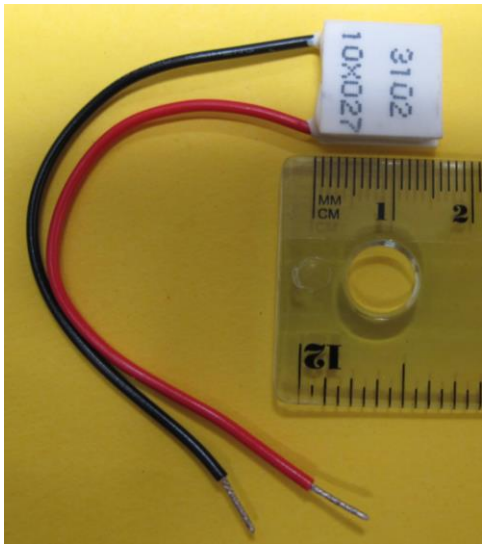

Figure 4.3 Photo of CP20151 Peltier Device

After the proof of concept test, the device was tested again as well as two other Peltier devices. The setup was the same as above with a different, warmer, person. The results show how power will differ under different conditions. Both tests were taken under normal conditions. Therefore, when this system is applied to an astronaut, variations should be expected.

Device Part #	Max V_{oc}	Max I_{sc}	Max P
CP20151	69 mV	5.6 mA	390 µW
CP60133	48 mV	4.1 mA	200 µW
G3-30-0508223	61 mV	4.4 mA	270 µW

Table 4.3 Three Energy Harvesters Initial Test

From these data sets it can be inferred that a single Peltier device will not produce enough power for a sensor; however, they could be used as a set in series and/or to charge a battery or supercapacitor, allowing intermittent transmit/receive operation of the radios which draw up to 100 mW when active.

4.3.5 Thermal Model of TEG in Spacesuit

Regardless of the perspective taken on human body it is challenging to model. The schematics below attempt to simplify the complex system. Thermal Model I assumes the TEG is integrated onboard. Thermal Model II assumes the TEG is off board. At this time both concepts remain options; however, the onboard option is more appealing—since it require less space.

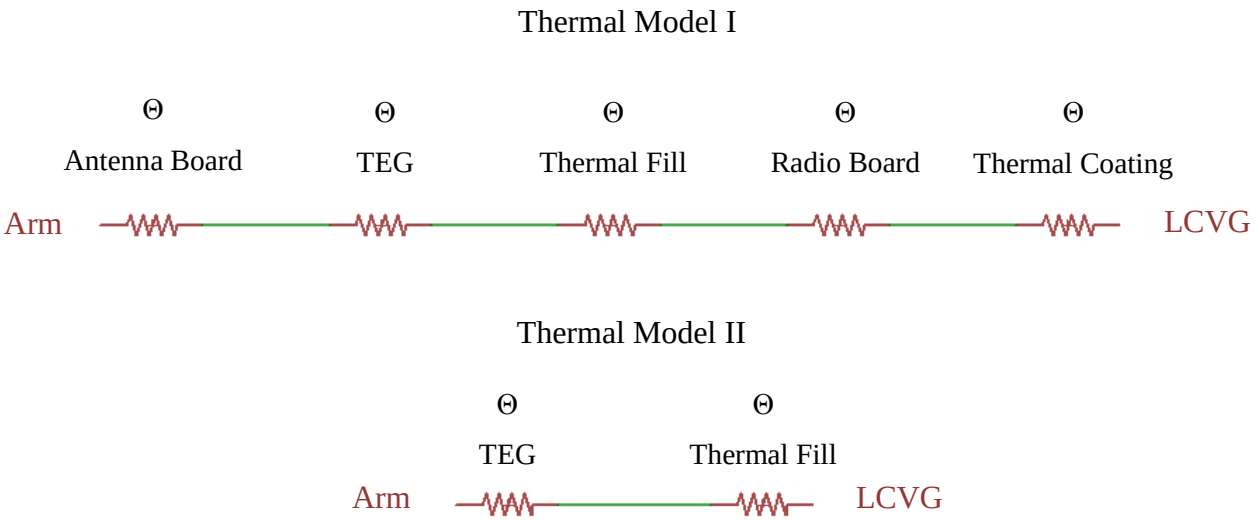

Figure 4.4 Thermal Models

Assuming, as suggested in [5], that the average person has a metabolism of 70 W/m^2 it is easy to upper bound the power input to a TEG with a known area. Two of the three TEGs used in this research have an area of 2.25 x 10^4 m^2 (15 mm x 15 mm). Thus the power into the TEG is 16 mW (this power is part of the thermal model—represented by a current source between the arm and LCVG). The next section looks at the power output for the generator from which the efficiency can be evaluated. In the model above θ represent the thermal resistance of each element between the arm and the LCVG. There is a ΔT across all of these elements. The relationship between thermal resistance, temperature across, and power is expressed as:

$$\theta_a = \frac{\Delta T_a}{P_{in}} \quad (4.1)$$

In this equation θ_a represent the thermal resistance across element a, ΔT_a represent the change in temperature across element a, P_{in} represents the input power (about 16 mW). If either the thermal resistance or the temperature across an element is known the other can be calculated. Ideally, θ_{TEG} would be the largest value in the series of thermal resistances. A large θ_{TEG} means most of power is input to the TEG thus producing the maximum voltage and power outputs.

4.4 Testing the Thermoelectric Generators

4.4.1 Test Setup and Procedures

To evaluate the three devices and to better understand the effects of various temperature differences, an experiment was designed. The cold side of the device under test (DUT) would remain at a constant room temperature while the hot side is adjusted using a 1°C step size. The open circuit voltage and short circuit current are measured using a digital multimeter. When measuring the current, the highest current level (10 A) is used. While this reduces the number of significant digits it ensures that the smallest resistance is used in the measurement.

A hot plate was used for this test so the temperature could be precisely controlled. Before starting the tests the hot plate would need a chance to equalize to room temperature. The equalization process took anywhere from a couple hours to an entire afternoon. This difficulty may be caused by the fickleness of Kansas weather.

During the test, the DUT was placed on a hot plate, hot side down. A heat sink with fan was connected to the cold side. A digital multimeter was connected to the two terminals of the DUT and alternated reading voltage and current. After the system had equalized and the voltage output was between -1 and 1 mV the test could begin.

The hot plate used is a TP294-C4 from Sigma System Corporation. The temperature is adjusted in five simple steps. The hot plate keypad interface makes these steps clear, using the numbers 1-5 next to the buttons to be used. Figure 4.5 shows the test set up.

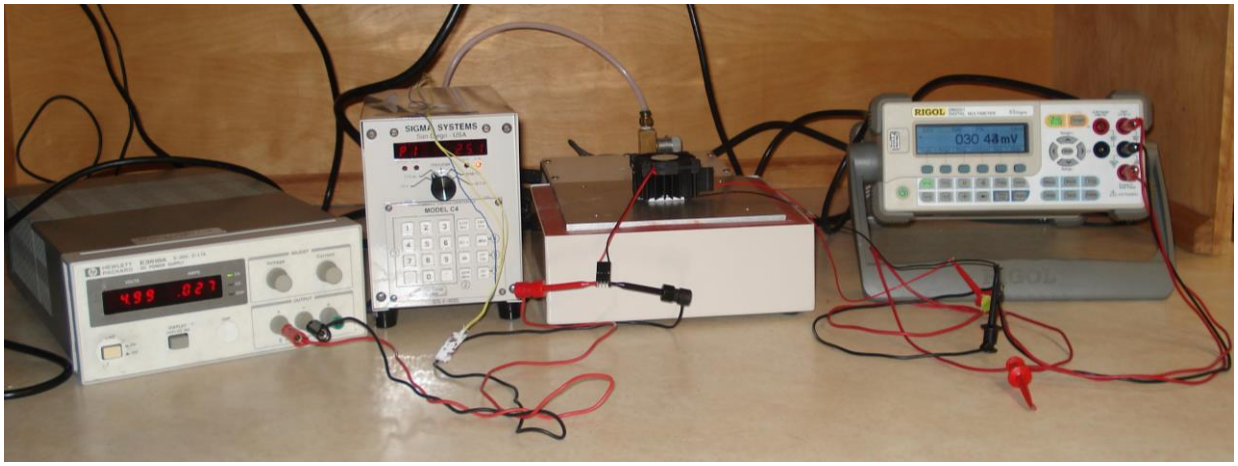

Figure 4.5 Energy Harvesting Test Set-Up

1. Press the display control button. This shows the current entry.
2. Press the clear entry button. This allows the entry to be set to the desired value
3. Press the 1 in the key pad. This sets the value for the sensor inside the plate. Then enter the desired temperature value, 1°C higher than the previous value. If the value is entered incorrectly return to step 2 and proceed normally.
4. Press the enter button. This will program the value.
5. Press the display temperature button. This will display the current temperature so the user knows when the desired temperature is achieved.

For the first time only the start button needs to be pushed. This tells the system that the temperature will be modified. Repeat steps 1-5 until the final temperature of interest (20°C higher than the base temperature) is reached. The following section details the test results.

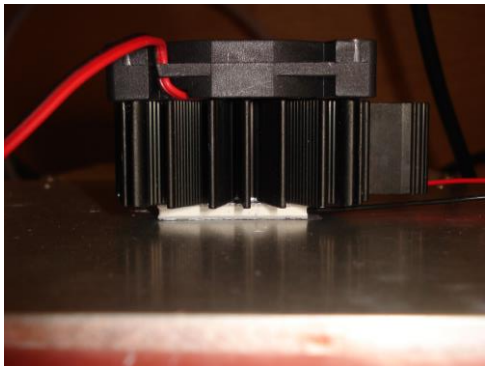

Figure 4.6 Close Up of TEG on Hot Plate with Heat Sink and Fan

Device Part #	Length and Width	Height
CP20151	15 mm	5.1 mm
CP60133	15 mm	3.3 mm
G3-30-0508223	30 mm	3 mm

Table 4.4 TEG Demensions

4.4.2 Test Results

The three different devices were tested on different days. The base-line temperature was not consistent; however, the range of temperatures and step size remained constant. The tables of values can be found in Appendix C. The following graphs illustrate the change in voltage, current, and power outputs as the difference in temperature increases. As expected voltage, current, and power all increase as ΔT increases It is interesting to note that for all three devices the voltage characteristics are fairly similar with CP20151 and CP60133 being nearly identical. In terms of current, G3-30-0508223 exhibits more of a parabolic behavior at larger temperature differences. The power graph is a combination of the previous two graphs and therefore continues to show the difference in terms of current.

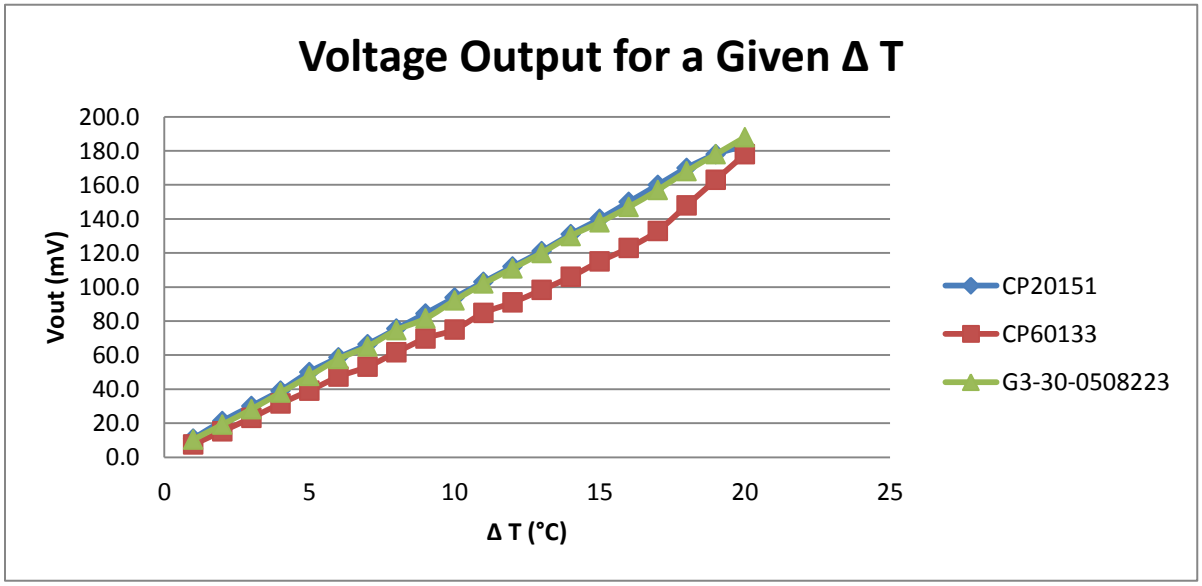

Figure 4.7 Energy Harvesting Voltage Output for a Given ΔT

These results are consistent with the room temperature plate and arm measurements in section 4.3.4. When combined they seems to indicate that the difference between skin and room temperature is around 5°C. As expected small temperature differences result in lower power output. Section 4.5 addresses this issue in more detail and provides a prototype solution.

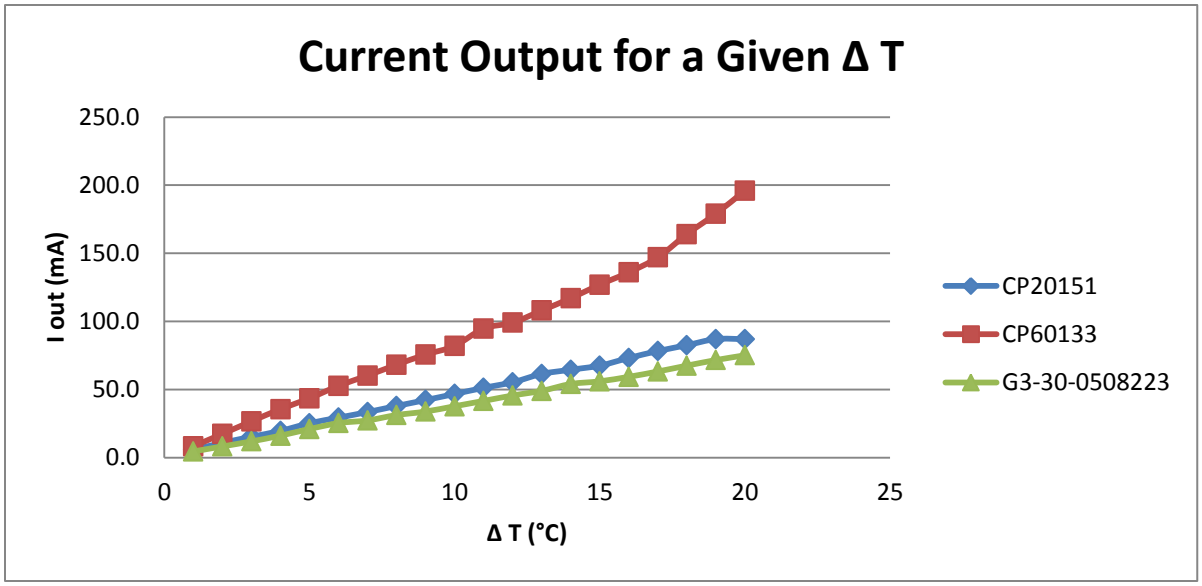

Figure 4.8 Energy Harvesting Current Output for a Given ΔT

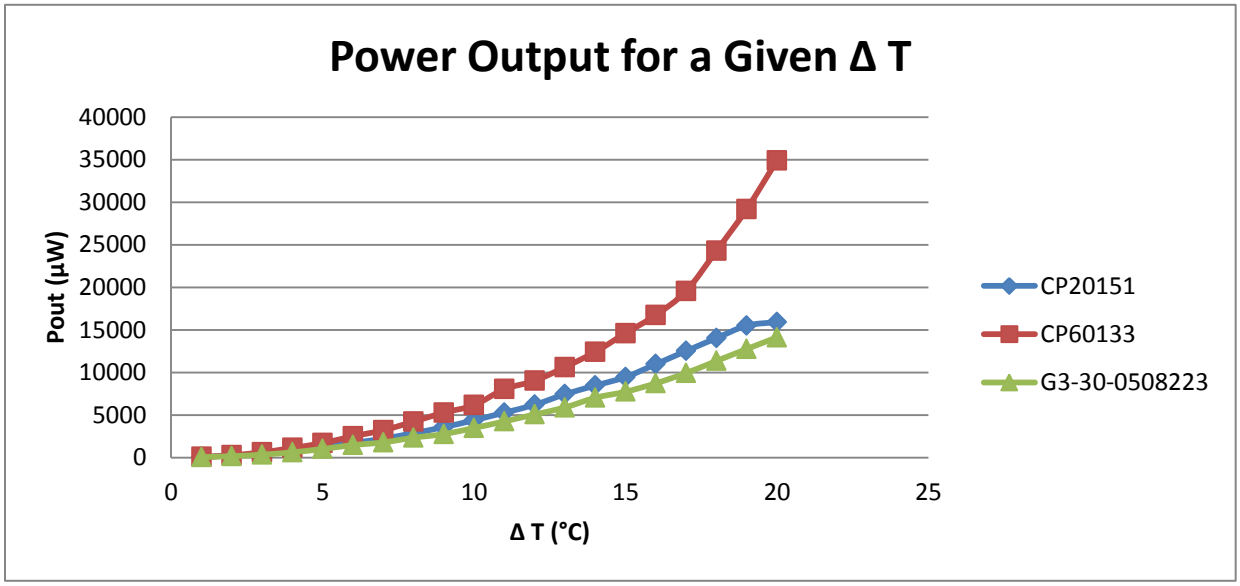

Figure 4.9 Energy Harvesting Power Output for a Given ΔT

These graphs show the increase in current with increased time. The CP60133 is capable of producing a larger current. However, in the range of temperature difference expected in the suit there is little advantage to using this device. The power graph is more telling of the minimal variation among the three TEGs. Regardless of which of the three is selected the power output is below 5 mW. Comparing this with the harvested power levels in table 4.3, we can infer that thermal resistance must play a large part in determining the power production and efficiency.

4.5 Energy Harvesting Low Voltage and Power Output Problem.

4.5.1 Understanding the Problem

As seen in the previous two sections, the power output from a thermoelectric generator is very small. The device alone would be unable to power a sensor, and in the case of radio burst communications the duty cycle would require a large charging time with a very short transmit time. When the thermoelectric generator is added to the existing radio with a super capacitor for storage there will also be issues charging the cap to an appropriate voltage.

4.5.2 Finding a Solution

There are two main ways to combat the low voltage and power output: using multiple TEGs electrically in series and/or finding a boost converter capable of working with 50 mV to 100 mV input. The first option is fairly simple and easy to implement since it only requires additional TEGs. On the negative side, the first option requires more space. Two devices remain reasonable but, based on voltage measurements, about 20 TEGs would be needed to achieve 1 V and require at least a 45 cm^2 surface area. Thus a better option is to use boost circuitry.

It took many internet searches to find a circuit which might be capable of boosting 50 mV to 5 V. Very few circuits are capable or starting up with such a low voltage. Fortunately, when evaluating some other options, we found Linear Technology LTC3108 Ultra low Voltage Step-Up Converter. This device was designed for energy harvesting. After reviewing the data sheet the integrated circuit and a few additional components recommended in the data sheet (Coilcraft Coupled Inductor LPR6235-752SML and CUI Inc. TEG CP60133) seemed to be an ideal solution.

4.5.3 Prototyping the Circuit

Before implementing the circuit as part of the entire system it was important to understand its operation. To this end the circuit was put together on a proto board. There are three main components to the circuit: the TEG, coupled inductors, and the ultralow voltage step-up converter and power manager IC.

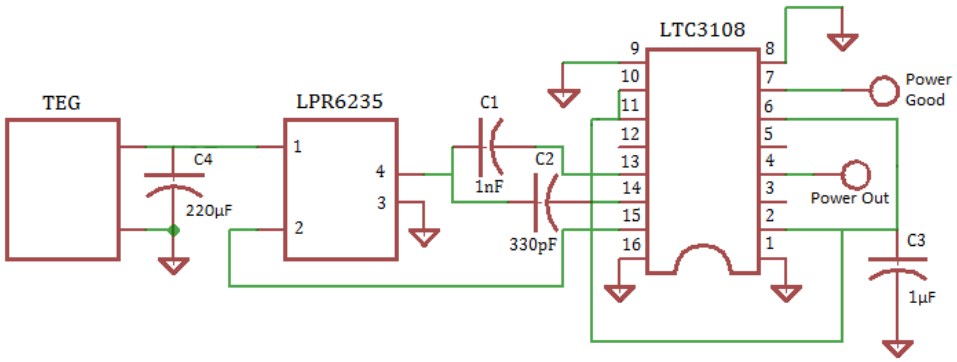

Figure 4.10 Schematic for Energy Harvesting Boost Circuit

This initial prototype was designed to provide a 5V output. Pins 10 and 11 set the voltage. There are four possible voltage settings. This one was initially selected because it provided the highest voltage. Most of the capacitor values are based off the IC's datasheet. The LPR6235 coupling inductors were also recommended on the datasheet.

4.5.4 Initial Testing of Prototype

Only the CP20151 TEG was tested with this system. Tests were done the same way as the initial concept test. The metal plate was placed on a table with the TEG on top, cool side down. The wrist was then placed on the top, hot side, of the TEG. An oscilloscope was used to read the output voltage—which also allowed for checking the voltage before and after the coupling inductors. As this was demonstrated in a project team meeting, many team members were used to verify the system's function. Most were able to supply the needed temperature to produce the 5 V output. The time before this voltage was reached varied with each individual. Of those that were unable to produce a voltage, this author believes that given more time the system would be able to charge and deliver the desired voltage. It should also be noted that the output node was not loaded during the test. Thus it is unclear how much current the system is capable of delivering. Future tests will be needed to evaluate this functionality, but it is recommended that at least two TEGs be used to provide a more robust solution.

Chapter 5 - Conclusion and Future Direction

5.1 Summary of Work

This thesis lays the ground work for the development of a daughter board for the micro-transceiver. A top hat antenna was selected based on its ability to meet the in-suit needs. Design constraints were derived from the size of the existing radio board and simulations of variation in top hat size, post height and post diameter. The top hat size was set by the size of the radio board. In a battery operated system, the radio board would become the top hat while the daughter board and the arm would be the ground. The height was also restricted by the connector used on the radio board. The resulting short height is actually beneficial as it leads to a smaller reactance magnitude and reduces the mismatch. A larger post diameter was also chosen as it would keep the physical resistance lower. After the antenna was designed and built, it was tested to find a matching network. From these tests S_{11} was found to vary dramatically inside the model suit. This leads to the conclusion that a perfect match could not be made. However, and imperfect match would still improve the efficiency of the antenna.

Two spacesuit models were used to test the antennas and get initial experimental estimates of path loss. Early in this testing a problem arose. The cable used to feed the antenna signal to a spectrum analyzer was functioning as part of the antenna. To alleviate this problem a wireless test solution was devised. A commercially available radio with a received signal strength indicator was used with an audio oscillator. The audio frequencies were mapped to power levels. The antennas were placed at a variety of locations on the body and test results indicate that regardless of a sensors location, the signal should be strong enough to be received by a wired link on the chest or back.

Finally, this work explored energy harvesting and how it could be implemented in the suit. Thermal energy harvesting seemed the most promising for the application. Three different thermoelectric generators (TEGs) were purchased and tested with temperature variations ranging from 0-20° C. It was found that a single TEG would not provide enough voltage for the supercap on the radio board. An ultralow voltage step-up converter and power manager was found and prototyped. This small IC and associated circuitry was able to supply a constant 5V after a short delay time.

5.2 Future Work

The antenna work on this project is fairly complete. A matching network should be implemented to improve efficiency. The original antenna design included pads for an L match so the future work is selecting the inductor and capacitor to be used. This antenna is the foundation of the daughter board. The additional components will be integrated into a modification of the antenna board discussed in Chapter 2.

The energy harvesting studied in Chapter 4 will be added to the antenna board. Current plans are to have two TEGs both fed to the boost circuit. Xiongjie Dong is designing a daughter board which will integrate these components and include a biosensor. The sensor to be incorporated is still being discussed. By the end of summer, Xiongjie plans to have the first rev of the daughter board complete.

Signal propagations studies are continuing. This summer a team of undergraduate students are testing radios at four different frequencies to better understand the suit environment. They are using procedures established in this text. The team's goal is to determine which of the frequencies behaves best in the suit.

Finally, further research should be done on the effect of coax cables on antenna measurements. The coupling issues expressed in Chapter 3 should be explored in depth to insure the accuracy of antenna measurements.

Bibliography

[1] "Medical Device Radiocommunications Service (MedRadio)." Internet: http://www.fcc.gov/encyclopedia/medical-device-radiocommunications-service-medradio [May 3, 2013].

[2] Yoo Sungjong; K.L. Melde, "VHF Collar Integrated Antenna for Ground Link of GPS Based Location System," Antennas and Propagation, IEEE Transactions on , vol.61, no.1, pp.26,32, Jan. 2013. http://ieeexplore.ieee.org/stamp/stamp.jsp?tp=&arnumber=6272328&isnumber=6397624

[3] K. Ito; N. Haga; M. Takahashi; K. Saito, "Electric field distributions around the human body with a small antenna in the frequency range of 2.5 MHz to 2.5 GHz," *Antenna Technology, 2009. iWAT 2009. IEEE International Workshop on* , vol., no., pp.1,4, 2-4 March 2009. http://ieeexplore.ieee.org/stamp/stamp.jsp?tp=&arnumber=4906966&isnumber=4906863

[4] Xiaoyu Cheng; D. E. Senior; Cheolbok Kim; Yong-Kyu Yoon, "A Compact Omnidirectional Self-Packaged Patch Antenna With Complementary Split-Ring Resonator Loading for Wireless Endoscope Applications," *Antennas and Wireless Propagation Letters, IEEE* , vol.10, no., pp.1532,1535, 2011. http://ieeexplore.ieee.org/stamp/stamp.jsp?tp=&arnumber=6111431&isnumber=5730210

[5] D.C. Hoang; Y.K. Tan; H. B. Chng; S. K. Panda, "Thermal energy harvesting from human warmth for wireless body area network in medical healthcare system," *Power Electronics and Drive Systems*, 2009. PEDS 2009. International Conference on , pp.1277,1282, 2-5 Nov. 2009. http://ieeexplore.ieee.org/stamp/stamp.jsp?tp=&arnumber=5385814&isnumber=5385648

[6] V. Leonov, "Thermoelectric Energy Harvesting of Human Body Heat for Wearable Sensors," *Sensors Journal, IEEE* , vol.13, no.6, pp.2284,2291, June 2013. http://ieeexplore.ieee.org/stamp/stamp.jsp?tp=&arnumber=6479224&isnumber=6504509

[7] X. Lu; S. H. Yang, "Thermal energy harvesting for WSNs," *Systems Man and Cybernetics (SMC), 2010 IEEE International Conference on* , vol., no., pp.3045,3052, 10-13 Oct. 2010. http://ieeexplore.ieee.org/stamp/stamp.jsp?tp=&arnumber=5641673&isnumber=5641665

[8] Y.K. Tan; S. K. Panda, "Energy Harvesting From Hybrid Indoor Ambient Light and Thermal Energy Sources for Enhanced Performance of Wireless Sensor Nodes," *Industrial Electronics, IEEE Transactions on* , vol.58, no.9, pp.4424,4435, Sept. 2011. http://ieeexplore.ieee.org/stamp/stamp.jsp?tp=&arnumber=5675682&isnumber=5979518

[9] "Design of Microwave Circuits," Class notes for ECE 764, Department of Electrical and Computer Engineering, Kansas State University, 2012.

[10] L. Greetis; R. Ouedraogo; B. Greetis; E. J. Rothwell, "A Self-Structuring Patch Antenna: Simulation and Prototype," *Antennas and Propagation Magazine, IEEE* , vol.52, no.1, pp.114,123, Feb. 2010. http://ieeexplore.ieee.org/stamp/stamp.jsp?tp=&arnumber=5466405&isnumber=5466383

[11] Wang-Ta Hsieh; Jean-Fu Kiang, "A Small Broadband Folded-Loop Antenna With Disk-Loaded Monopole," Antennas and Wireless Propagation Letters, IEEE , vol.9, no., pp.1248,1250, 2010. http://ieeexplore.ieee.org/stamp/stamp.jsp?tp=&arnumber=5688278&isnumber=542332

[12] E. Ghafari; D. N. Aloi, "Top-loaded UWB monopole antenna for automotive applications," Antennas and Propagation Society International Symposium (APSURSI), 2012 IEEE , vol., no., pp.1,2, 8-14 July 2012. http://ieeexplore.ieee.org/stamp/stamp.jsp?tp=&arnumber=6347985&isnumber=6347935

[13] V. Trainotti; L. A. Dorado, "Short low- and medium-frequency antenna performance," Antennas and Propagation Magazine, IEEE , vol.47, no.5, pp.66,90, Oct. 2005. http://ieeexplore.ieee.org/stamp/stamp.jsp?tp=&arnumber=1599168&isnumber=33625

[14] M. Deutch, W. Hanson, G. Nelson, C. Snider, D. Sutton, W. Yates, "WWVB Improvements: New Power from an Old Timer" Time and Frequency Division NIST. Boulder, CO, Tech. Rep.

[15] G. Nelson. "RE: WWVB Antenna Dimensions." Personal email (May 23, 2013).

[16] ILC Dover. "Space Suit Cross Section" Documentation included with sample of suit.

[17] M. Taj-Eldin; W. B. Kuhn; B. Natarajan, "Performance Evaluation of Radio Channel for Astronaut Body Area Networks" unpublished.

[18] Parallax INC. "433 MHz RF Tranceiver" [online], Nov. 2009. Available: http://www.wulfden.org/downloads/manuals/27982-433MHzRFTransceiver-v1.1.pdf.

[19] Linx Technologies. "LT Series Transceiver Module" [online], March 2010. Available: http://datasheetz.com/data/RF%20and%20RFID/RF%20Transceiver%20ICs%20and%20Modules/TRM-433-LT-datasheetz.html.

[20] A. D. Joseph, "Energy harvesting projects." *Pervasive Computing*, IEEE, vol.4, no.1, pp.69,71, Jan.-March 2005. http://ieeexplore.ieee.org/stamp/stamp.jsp?tp=&arnumber=1401845&isnumber=30432

[21] H. M. G. E. D. M. El-Anzeery; M. A. E. A S. El-Bagouri; R. Guindi. "Novel radio frequency energy harvesting model." Paper presented at *Power Engineering and Optimization Conference (PEDCO)* Melaka, Malaysia, 2012 IEEE International, vol., no., pp.209,213, 6-7 June 2012. http://ieeexplore.ieee.org/stamp/stamp.jsp?tp=&arnumber=6230862&isnumber=6230825

[22] “Research-Power and Energy Systems.” Internet: http://ece.ksu.edu/research-power-and-energy-systems [May 16, 2013].

[23] X. Zhang. “UHF & UHF Energy Harvesting Radio System Physical and MAC layer Considerations.” M.S. thesis, Kansas State University, Manhattan, Kansas, 2009.

[24] M. R. Mhetre; N. S. Nagdeo; H. K. Abhyankar, “Micro energy harvesting for biomedical applications: A review.” Paper presented at *Electronics Computer Technology (ICECT),* 2011 3rd International Conference on, vol.3, no., pp.1,5, 8-10 April 2011. http://ieeexplore.ieee.org/stamp/stamp.jsp?tp=&arnumber=5941789&isnumber=5941735

[25] A. C. Guyton. “Body Temperature, Temperature Regulation, and Fever" in *Textbook of Medical Physiology*, 8th ed. W. B. Saunders, Ed. Philadelphia: Harcourt College Pub, 1991, pp. 797-808.

[26] G. Sanchez. “Up-To-Date Report.” Personal email (Aug. 1, 2012).

[27] “AOL.on Perpetua Tegwear First Look.” Internet: http://on.aol.com/video/perpetua-tegwear-first-look-517638331[May 10, 2013].

Appendix A - ADS Simulation Tutorial

A.1 Building the Antenna

All simulations were done in ADS 2009. I started a new project, named it, and selected mils for units. A help window will appear. Depending on the users comfort level with ADS, the user can decide to use the help prompt. After exiting the help window the Schematic window will open. In this project the focus is on layout so the Schematic window is closed and from the top menu select Layout>>Generate/Update Layout. The antenna will be implemented in the Layout window.

The three components are required for the simulation set up: the top hat, the post and a base—the base in used to attach the port and acts as the excitation point. Using the circle feature on the tool bar creates the post. After selecting the tool, click on the center of the layout (0,0) and pull the mouse until reaching the desired radius (75 mills). Set the layer type by double clicking on the circle. The properties box will appear; change the layer to diel (for dielectric—note: the layer is only dielectric for simulation purposes) and click OK. The square base is 10 mills wider than the post. Select the rectangle tool. Start from (-80, 80) and drag to the opposite corner (80, -80). Again, the layer will need to be changed, this time to cond2. The final top hat component is created using the circle as with the post. This circle will be larger (500 mil radius); however, the steps are the same as before—select the circle tool, start from (0, 0) and drag to the desired radius size. The layer should be cond. The antenna is now ready for simulation—discussed in section A.2. In a latter section, Adjusting Parameters, we will see how to change parameters if they are not the desired values.

A.2 Setting up for Simulation

Before running a simulation a few parameters need to be set or modified. Additionally there are two different simulations options: FEM (Finite Element Method) or Momentum. The configuration for both simulations follows the same steps and both were used in this research. The author has chosen to focus on FEM. To set up and FEM simulations select FEM from the top menu bar. From the submenu select Substrate >> Create/Modify . This sets up the layers for simulation. In the substrate layer tab, change Alumina to Air. Change the thickness to the

desired post height value, 500 mils as base case, and the permittivity to 1. Add another layer. Call it FR4 and enter a thickness of 62 mils and a permittivity of 4.6.

In the same window select the layout layers tab. The top bashed line should be cond. Select the layer and change the Layout Layer Name to cond (the top hat layer), then chose strip. For the second dashed line changed the Layout Layer Name to cond2 (the base layer) also choosing strip. The Air layout layer should be diel, select via (it's the only option). (NOTE: diel is short for dielectric. This may cause some initial confusion, as the post is metal. However, the air gap between the base and top hat performs the same functions as the dielectric of a parallel plate capacitor—thus creating a capacitive loaded antenna.). While setting up these characteristics, notice the Material section. Initials runs used only perfect conductors: however, in later runs these characteristics can easily be modified (see next section).

Finally, the port is placed. Use the port symbol on the toolbar. Select cond2 (the base) for the layer and click okay. Place the port on the edge of the base, just touching the edge. In the top menu bar, select FEM >> Ports. Select the port in the layout, then click apply. The simulation is ready to be run.

There are a few additional steps involved in setting up the simulation itself. To run the simulations select FEM from the top menu bar. From the submenu select Simulate >> S-Parameters (this research looked primarily at S_{11}). A simulation window will pop up. To keep the run time short select single from the drop down sweep type. Set the desired Frequency, 400 MHz in these experiments. Click apply, then simulate and wait for the program to run.

When the simulation is complete the graphs will pop up. Delete the phase and magnitude graphs. The Smith Chart provides the data of interest. Next, select marker >> new from the menu bar. Place the marker on the point to display its impedance. The impedance will be normalized. To denormalize it double click in the box containing the marker data. In the format tab change Z_0 to 50 Ohms and click okay.

A.3 Adjusting Parameters

To understand the role of each parameter, I adjusted one while the other two remained constant. This section outlines how to change all three parameters once the initial antenna layout is complete. The height of the post is determined by the Air gap between the FR4 layers. To change it, go to FEM >> Substrate >> Create/Modify . . . . In the Substrate Layers tab select Air

and change the thickness to the desired height. The top hat diameter is determined by the radius of the circle. To change it, double click on the circle in the layout. The properties window should appear. Change the radius to give the desired diameter. Similarly, the post diameter can be changed using the same steps. Resize the circle by double clicking and changing the radius to produce the desired diameter. After resizing the circle representing the post, the base should also be adjusted. Double click the square base to get the properties window. Change the Lower Left X and the Lower Left Y to the negative radius minus five (i.e. if the radius was 10 mils the Lower Left X and Y should be -15 mils). Also, change the Height and Width to the diameter plus ten.

Appendix B - K-State Microtransceiver Radio Photos

The following images are included to provide an understanding of the daughter board's design. Figure B.1 shows the board size relative to the human arm. The U.Fl connecter on the left of the board is for the antenna connection. There is also a pad on the bottom of the board which will be used for the top hat antenna. Figure B.2 is included to illustrate how the daughter board will connect with the mother radio board. In the picture the bottom board is a break out board used for programing signal processing components.

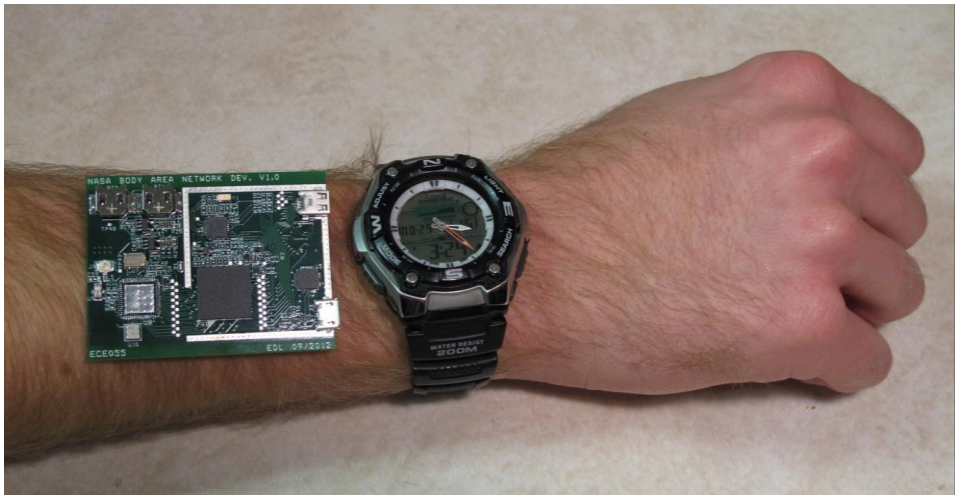

Figure B.1 Microtransceiver Radio on Arm

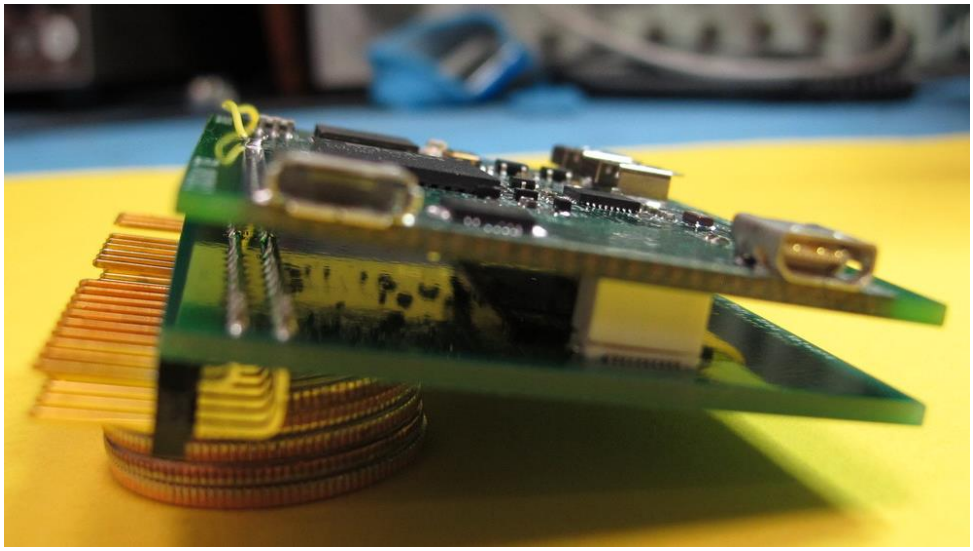

Figure B.2 Microtranseiver Radio Board with Breakout Board (same size and connection as daughter board)

Appendix C - Energy Harvesting Device Tables

The following tables are the numerical data expressed graphically in section 4.4.2. Each table contains data for a single thermoelectric generator (TEG) with temperature differences from 1 to 20. Voltage and current were measured using a digital multimeter (DMM). The power was calculated based on the voltage and current outputs.

plate temp (°C)	Δ temp (°C)	Output Voltage (mV)	Output Current (mA)	Output Power (μW)
26.7	1	11.0	5.8	63.8
27.7	2	21.3	10.8	230
28.7	3	30.1	15.3	461
29.7	4	39.2	19.6	768
30.7	5	50.1	25.2	1,263
31.7	6	58.6	29.3	1,717
32.7	7	66.4	33.4	2,218
33.7	8	75.5	37.9	2,861
34.7	9	84.5	42.2	3,566
35.7	10	93.8	46.7	4,380
36.7	11	103	51.2	5,274
37.7	12	112	55.3	6,194
38.7	13	121	61.4	7,429
39.7	14	131	64.5	8,450
40.7	15	140	67.5	9,450
41.7	16	150	73.1	10,965
42.7	17	160	78.2	12,512
43.7	18	170	82.5	14,025
44.7	19	178	87.0	15,486
45.7	20	183	87.0	15,921

Table C.1 Output for CP20151 TEG for a Given ΔT

plate temp (°C)	Δ temp (°C)	Output Voltage (mV)	Output Current (mA)	Output Power (µW)
24.1	1	7.5	8.3	62.25
25.1	2	15.3	17.4	266
26.1	3	23.1	26.6	614
27.1	4	31.5	35.6	1,121
28.1	5	39.1	43.5	1,701
29.1	6	47.3	52.7	2,493
30.1	7	53.2	60.2	3,203
31.1	8	61.7	68.2	4,208
32.1	9	69.8	75.6	5,277
33.1	10	75.0	82.0	6,150
34.1	11	84.8	94.7	8,031
35.1	12	90.9	99.1	9,008
36.1	13	98.3	108	10,616
37.1	14	106	117	12,402
38.1	15	115	127	14,605
39.1	16	123	136	16,728
40.1	17	133	147	19,551
41.1	18	148	164	24,272
42.1	19	163	179	29,177
43.1	20	178	196	34,888

Table C.2 Output for CP60133 TEG for a Given ΔT

plate temp (°C)	Δ temp (°C)	Output Voltage (mV)	Output Current (mA)	Output Power (µW)
24.6	1	10.4	4.5	46.8
25.6	2	19.2	8.2	157
26.6	3	28.2	11.9	336
27.6	4	37.9	16.1	610
28.6	5	47.8	21	1,004
29.6	6	57.7	25.3	1,460
30.6	7	65.0	27.3	1,775
31.6	8	74.7	31.2	2,331
32.6	9	81.5	33.8	2,755
33.6	10	92.1	37.7	3,472
34.6	11	102	41.6	4,243
35.6	12	111	45.6	5,062
36.6	13	120	49	5,880
37.6	14	130	54	7,020
38.6	15	138	56	7,728
39.6	16	147	59.3	8,717
40.6	17	157	63.2	9,922
41.6	18	168	67.5	11,340
42.6	19	178	71.6	12,745
43.6	20	188	75.1	14,119

Table C.3 Output for G3-30-0508223 TEG for a Given ΔT